Mechanistic Studies and Inhibition of N-hydroxylating Monooxygenases

Kendra Bufkin

Thesis submitted to the faculty of Virginia Polytechnic Institute and State University in partial fulfillment of the requirements for the degree of

Master of Science in Life Sciences

In

Biochemistry

Pablo Sobrado, Chair

Zachary Mackey, Committee Member

Robert H White, Committee Member

April 20, 2017

Blacksburg, VA

Keywords: AfSidA (*Aspergillus fumigatus* Siderophore A), AMO (*Amycolatopsis alba* monooxygenase), siderophore, flavin, hydroxylation

Mechanistic Studies and Inhibition of N-hydroxylating Monooxygenases

Kendra Bufkin

Abstract

N-hydroxylating monooxygenases (NMO) are members the class B flavoprotein monooxygenases. They catalyze the N-hydroxylation of lysine and ornithine and play and essential role in the biosynthesis of hydroxamate containing siderophores. Siderophores are high affinity iron-chelators composed of catechol and hydroxamate functional groups that are synthesized and secreted by several microorganisms and plants. It has been showed that many NMOs are essential for virulence in many opportunistic pathogens such as *Aspergillus fumigatus* and *Pseudomonas aeruginosa.* The focus of my research is on the N-hydroxylating enzymes: Siderophore A (SidA) from *Aspergillus fumigatus* and *Amycolatoposis alba monooxygenase* (AMO).

One of my projects is focusing on identifying inhibitors of SidA that will ultimately block the siderophore biosynthesis in *A. fumigatus.* Out of 973 compounds screened using an activity high-throughput assays two compounds were identified. These were, wortmannin a steroid metabolite and ebselen a benzoselenazole as SidA inhibitors with IC_{50} values of 369 μM and 11 μM respectively. A second part of this works investigates the hydroxamate formation of the siderophore albachelin in *Amycolatoposis alba* with the purpose of better understanding this class of enzymes and their catalytic mechanism. The enzyme was purified and characterized in its holo (FAD-bound) and apo (unbound) forms. Pre-steady and steady state kinetics shows that the two forms have different coenzyme preference; apo-AMO prefers NADH while holo-AMO has a higher affinity to NADPH.

Mechanistic Studies and Inhibition of N-hydroxylating Monooxygenases

Kendra Bufkin

General Audience Abstract

N-Hydroxylating monooxygenases (NMOs) are unique class of enzymes which are involved in the production of small iron binding molecules known as siderophore. Siderophores are used by some fungi and bacteria to acquire iron from the human host during infection. This thesis focuses on the inhibition and characterization of Siderophore A (SidA) from *Aspergillus fumigatus* and *Amycolatopsis alba* monooxygenases (AMO). SidA is an enzyme of interest because it is required for siderophore production and has been shown to be required for pathogenesis in *A. fumigatus.* In this thesis, a drug-discovery processes known as high-throughput screening was used to identify potential inhibitors of SidA. Using a several other assays, two compounds were validated as inhibitors of *A. fumigatus*.

In addition, this work also investigates the reaction of AMO by focusing on the different stages of the enzyme mechanism; such as oxygen consumption, product formation, and flavin reduction. Overall, the goal of this thesis is to provide insight into the N-hydroxylating monooxygenases class of enzymes as well as to find new compounds that can lead to the next generation of antifungal drugs.

Acknowledgements

I would like to thank my Heavenly Father for his grace and giving me the strength to complete this degree. I extend my most sincere gratitude to my advisor Dr. Pablo Sobrado for all his support, guidance and patience. I am grateful to my committee members Dr. Zachary Mackey and Dr. Robert H. White for their time and advice in the improvement of my research skills.

To each member of the Sobrado lab: Dr. Julia Del Martin-Campo, Dr. Meital Eckshtain Levi, Didier Mena Aguilar, Han Nam and Hannah Valentino for their assistance, valuable input and friendship. I am also thankful for Dr. Nancy Vogelaar for her support and assistance during the high throughput screening assays. I would also like to thank the Virginia Tech IMSD and George Washington Carver program for all their support and funding.

Finally, I would like to thank to my parents, my brother and friends for all their endless love, support and motivation in diverse ways in the completion of my Master degree.

Table of Contents

Chapter 1: Introduction

1.1 Flavoenzymes

Flavoenzymes play a significant role in aerobic metabolism because of their capability to catalyze one and two electron transfer reactions. They contain either FAD or FMN as a cofactor and they are highly enantio and regio-selective. Their mechanistic properties are also important for industrial biocatalytic applications such as prodrug activation (1), antibiotic synthesis (2) and production of enantiopure fine chemicals (3). Many of them are from bacterial origin and can be easily overexpressed in recombinant forms (4). Flavoproteins oxidases and monooxygenase have gain interest because of their regio-selective characteristics. This thesis will focus on flavin-dependent monooxygenases.

1.2 Flavin Dependent Monooxygenases

Flavin dependent monooxygenases are a unique class of enzymes that uses FAD/FMN as a cofactor (5). Over 130 of these enzymes have been characterized since the first flavin-dependent monooxygenase, lactate-2-monooxygenase was discovered in 1957 (5,6). Hydroxylation, epoxidation and Baeyer-Villiger oxidation are among the several types of oxygenation reactions catalyzed by flavin-dependent monooxygenase. Most monooxygenases require three substrates: NAD(P)H for flavin reduction, molecular oxygen, and a substrate that will be oxygenated. In these types of reactions, a single atom of oxygen is incorporated into the substrate, while the other oxygen atom is reduced to water (7). $C_{(4a)}$-hydroperoxyflavin (Figure 1) is a covalent adduct that serves as the oxygenating reagent. This intermediate can act as either a nucleophile or an electrophile depending on the terminal peroxide group protonation site (8). For electrophile substrates the oxygenating reagent is the peroxide and hydroperoxide for nucleophilic substrates (9). In general, the $C_{(4a)}$-hydroperoxyflavin specie is quite unstable and typically decays into hydrogen peroxide and oxidized flavin (10,11). However, properties of flavin monooxygenases make them effective enzymes for stabilizing this species and allowing $C_{(4a)}$-hydroperoxyflavin to oxygenate a substrate.

1.3 Classifications of Flavin Dependent Monooxygenase

Flavin dependent monooxygenases can be classified into six subfamilies. Classification of flavoenzymes are based on several characteristics such as amino acid sequence similarities, type of reaction catalyzed and the properties of the reducing/oxidizing substrates (12). Subfamilies A-B are composed of single component enzymes, compared to the two component enzymes found in families C-F where an NAD(P)H flavin reductase is needed for reduction of flavin. All classes are FAD-dependent, except the enzymes belonging to the subfamily C. A description of each class with their cofactor, reaction type and protein fold can be found in Table 1.

Class A flavoprotein monooxygenases are encoded by a single gene that can utilize either NADPH or NADH as co-substrates. They are composed of one dinucleotide binding domain for FAD binding. In this class $NADP^+$ is released immediately after reduction of flavin. Common substrates include aromatic compounds with an activating hydroxyl or amino group (4,13). The $C_{(4a)}$-hydroperoxyflavin intermediate acts as an electrophile while the substrate acts as a nucleophile. The prototype enzyme of this class is *p*-hydrobenzoate hydroxylase (PHBH) also known as 4-hydroxybenzoate-3-monooxygeanse (EC 1.14.13.2.) from *Pseudomonas* (11,14). Many members of class A are involved in microbial degradation that catalyze ortho or para hydroxylation of phenolic compounds (15).

Class B flavin monooxygenase can be further divided into three subfamilies: flavin-containing monooxygenases (FMOs), Baeyer-Villiger monooxygenases (BMVOs) and N-hydroxylating monooxygenase (NMOs). They contain two α/β Rossmann domains which are used for binding NADPH and FAD. One of the main differences between family A and B is that the pyridine nucleotide coenzymes is bound throughout catalysis, and the substrate does not bound until after the formation of the $C_{(4a)}$-hydroperoxyflavin in the group B flavin monooxygenase (13). The first crystal structure of a Group B flavin monooxygenase was solved in 2004 (16). Out of three types of reactions in the group B, the NMOs are the least studied and more specific because it is only present in bacteria and fungi. NMOs are involved in the biosynthesis of hydroxamate-based siderophores, deoxyribonulceotide synthesis, oxidative phosphorylation and electron transport in which they catalyze nucleophilic terminal amine groups of L-ornithine, L-lysine, and the primary aliphatic diamines such as 1,3-diaminipropane, cadaverine and putrescine (5). The role of NMOs in the biosynthesis of siderophores (iron chelators) is important to note because recently

siderophores and its biosynthetic pathways has been identified as potential targets to improve the diagnosis and treatment of fungal infections.

Class C monooxygenase are coded by multiple genes, where a TIM-barrel fold makes up the structural core. These types of enzymes utilize reduced FMN as the coenzyme which is generated by the reductase NAD(P)H (13). Bacterial luciferase (EC 1.14.14.3.) and alkane sulfonate monooxygenase (EC 1.14.14.5.) are two of the most well characterized enzymes of this class. Bacterial luciferase was the first flavoenzyme to show evidence of the $C_{(4a)}$-hydroperoxyflavin intermediate formation via NMR studies (5). Bacterial luciferase is unique because of its ability to emit light based on the oxidation of aliphatic aldehydes (17). Kinetic studies show that the transfer of reduced FMN between the reductase and luciferase happens through free diffusion (18). The two-component alkanesulfonate monooxygenase system catalyze carbon-sulfur bond cleavage in organosulfates to form aldehydes (11,14). The other three two-component flavoenzyme classes (D-F) are like Class C, however they utilize FAD as a cofactor. Class E and F have one nucleotide binding domain for FAD.

A

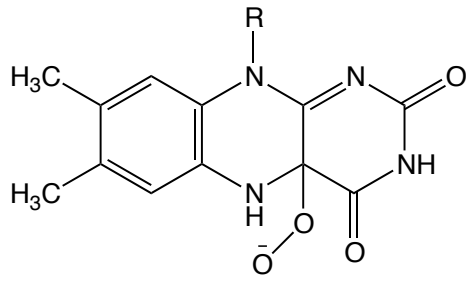

B

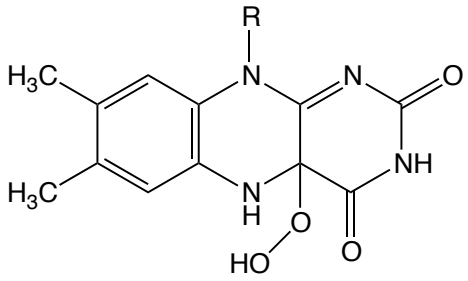

Figure 1: Chemical structures of the flavin C_{4a}-oxygen adduct: (A) C_{4a}-peroxyflavin and (B) C_{4a}-hydroperoxyflavin.

Table 1: Flavin-dependent monooxygenase classification.

Subfamily	Cofactor	Protein Fold	Reaction	Examples
A	FAD	Rossmann (Gr-2) [a]	Hydroxylation	*p*-hydroxybenzoate hydroxylase(11)
B	FAD	Rossmann (FMO) [b]	-Sulfoxidation -Baeyer-Villiger oxidation -N-hydroxylation -Heteroatom oxygenation -Oxidative decarboxylation	-Cyclohexanone monooxygenase(19) -L-Ornithine monooxygenase(20)
C	FMN	Tim-barrel	-Light emission -Baeyer-Villiger oxidation, epoxidation -Desulfurization, Sulfoxidation -Hydroxylation	Luciferase(13)
D	FAD/FMN	Acyl-CoA dehydrogenase	-N-hydroxylation -Hydroxylation	4-OH-phenylacetate hydroxylase(13)
E	FAD	Rossmann (Gr-2)	Epoxidation	Styrene monooxygenaase(21)
F	FAD	Rossmann (Gr-2)	Halogenation	Tryptophan-7-halogenase (22)

[a] GR- glutathione reductase
[b] FMO- flavin-containing monooxygenase

1.4 Siderophores

Siderophores are high-affinity iron chelators that are generally less than 1 kDa in size. These molecules are produced under iron limiting conditions by bacteria and fungi. The main role of siderophores is to scavenge iron from their environment and to make it available to microbial cells (23). In addition to this role, siderophores are involved in intracellular transport and storage of iron which is important for germination, asexual and sexual reproduction, antioxidative defense as well as virulence in plant and animal host (24).

Iron is the fourth most abundant transition metal in the Earth's crust but is not available at physiological pH. The insolubility of Fe(III) (K_{sp} of $Fe(OH)_3=10^{-39}$) at physiological pH in aerobic environment makes the bioavailability of this essential nutrient limited. Iron is an essential element for the growth of most bacteria and a key element in many biological and metabolic processes including deoxyribonulceotide synthesis, oxidative phosphorylation, methanogenesis and electron transport. The limited availability of Fe makes the development of iron acquisition pathways by pathogens necessary. Mammals sequester iron from Fe-binding proteins such as lactoferrin, transferrin and ferritin during infection as a defense mechanism (25). On the other hand, microorganism have developed siderophore–dependent iron uptake systems. The siderophore dependent iron acquisition pathways are present in several prokaryotic and eukaryotic systems. The common theme in siderophore dependent iron acquisition pathways is the production of one or more siderophores by cells upon iron starvation (26). Secreted siderophores scavenge Fe by forming a complex with Fe(III).

1.5 General Characteristics of Siderophores

Classification of siderophores is based on the chemical moieties that donates the oxygen ligands for Fe(III) coordination. Siderophores can be divided into three main classes: a) catecholates, b) hydroxamates and c) carboxylates (Figure 2). All three are coordinated differently to the Fe(III) metal.

Fungal hydroxamates siderophores includes four main families: rhodotorulic acid, fusarinines, coprogens and ferrichromes. The nitrogen of the hydroxamate group from all the fungal siderophores are derived from N^5-hydroxyornithine (27). The hydroxamate prosthetic groups requires N^5-acylation for completion. The octahedral complex of siderophores are

composed of three hydroxamate groups linked by peptide or ester bonds. The ferrichrome family are cyclic hexapeptides consisting of three N^5-acyl-hydroxyornithine and three amino acid combinations of alanine, serine or glycine (28). In contrast the fusarinines are comprised of three N^5-cis-anhydromevalonyl-N^5-hydroxyornithines which are linked by ester bonds.

1.6 Significance of Project

In this study, we focus on the biochemical characterization and inhibition of two enzymes belonging to flavin-dependent monooxygenases subclass B. These enzymes included Siderophore A from *Aspergillus fumigatus and Amycolatoposis alba* monooxygenase (AMO). Emphasis will be placed on the identification and characterization of inhibitors of the biosynthesis pathway of SidA using high throughput assays from two libraries: Kinase and a NIH collection library with a total of 973 compounds including natural products and market drugs. As well as the expression, purification and the pre-and steady-state kinetic characterization of AMO. This work will enable us to better understand the NMO class of enzymes and their mechanism of action. Thus, identifying inhibitors of SidA is an essential need to address the lack of specific pathogen drug targets and the current antibiotic crisis.

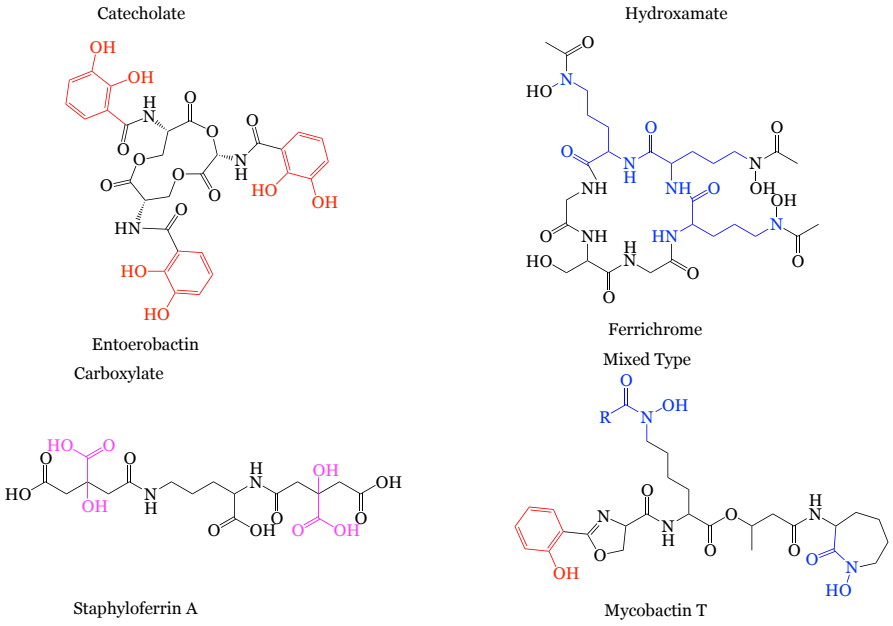

Figure 2: Chemical structures of the different classes of siderophores. Moieties involved in iron coordination are colored as follows: catecholates (phenolates) are in red, hydroxamates are in blue and carboxylates are in pink.

Chapter 2: Identification and Characterization of inhibitors of SidA

2.1 Introduction

One of the most well studied and characterized enzymes of class B is SidA, an N^5-ornithine hydroxylase from *A. fumgiatus*. SidA catalyzes the first committed step in the siderophore biosynthetic pathway of *A. fumgiatus* (Figure 3*)*. In this step ornithine is hydroxylated to N^5-hydroxyl-L-ornithine (29). The pathway continues by the transfer of acyl group from acyl-CoA derivatives to N^5-hydroxy-L-ornithine which allows the formation of the hydroxamate group. In *Aspergillus fumigatus* there are two transacylases SidF and SidL, which add two different acyl groups to hydroxyornithine (30). This step provides the foundation of the pathway split from nonribosomal peptide synthetases (NPRS) to allow the prefer acyl group to be chosen. Ferricrocin and ferrichrome are linked to acetyl while fusarinines and coprogens includes anhydromevalonyl (31). In ferrichromes an additional step is necessary for linking of the hydroxamate groups. This type of hydroxamates also uses NPRS for the incorporation of the three amino acid groups (32). SidD and SidC are the two NPRS involved in the synthesis of intra-extracellular siderophores in *A. fumigatus* (30).

Overall, the production of siderophores has gained a lot of attention because they often function as virulence factors in bacterial, pathogens and fungi species. Therefore, they are attractive targets in the development of new antimicrobial therapies for *Mycobacterium tuberculosis (33), A. fumigatus, Vibrio anguillarum* (34)*,* and *Pseudomonas aeruginosa* (35). It has been confirmed that L-ornithine-N^5-oxygenase is essential for infection in *A. fumigatus*. To uncover the importance of *sidA* in the siderophore biosynthetic pathway, a strain with the deletion of the *SidA* gene was constructed. The resulting mutant Δ*sidA* was unable to produce triacetylfusarinine C (TAFC), ferricrocin (FC) and unable to establish infection in mice (36).

The potential of the siderophore biosynthesis pathway of *A. fumigatus* to be a drug target was first reported in 2016, when a small molecule was identified as inhibiting this pathway. In this report, it was shown that celastrol a natural product can inhibit siderophore production and fungal growth. Celastrol completely abolished *A. fumigatus* growth at minimum inhibitory concentration of 2 μM in Aspergillus minimum media (AMM) without supplementation of iron (AMM-Fe). Docking studies suggest that celastrol targets SidA by occupying the NADPH binding site. Overall this study showed that inhibition of siderophore production prevents *A. fumigatus* growth under

iron-limiting conditions. This demonstrates that SidA and biosynthesis of siderophore is essential for *A. fumigatus* virulence. These studies provided the foundation and bases to develop new antifungal therapies targeting the siderophore acquisition system.

Therefore, this part of the thesis describes the identification and characterization of compounds that can inhibit the first step of the siderophore pathway of *A. fumigatus* by first using high-throughput screening assays to identify potential drugs.

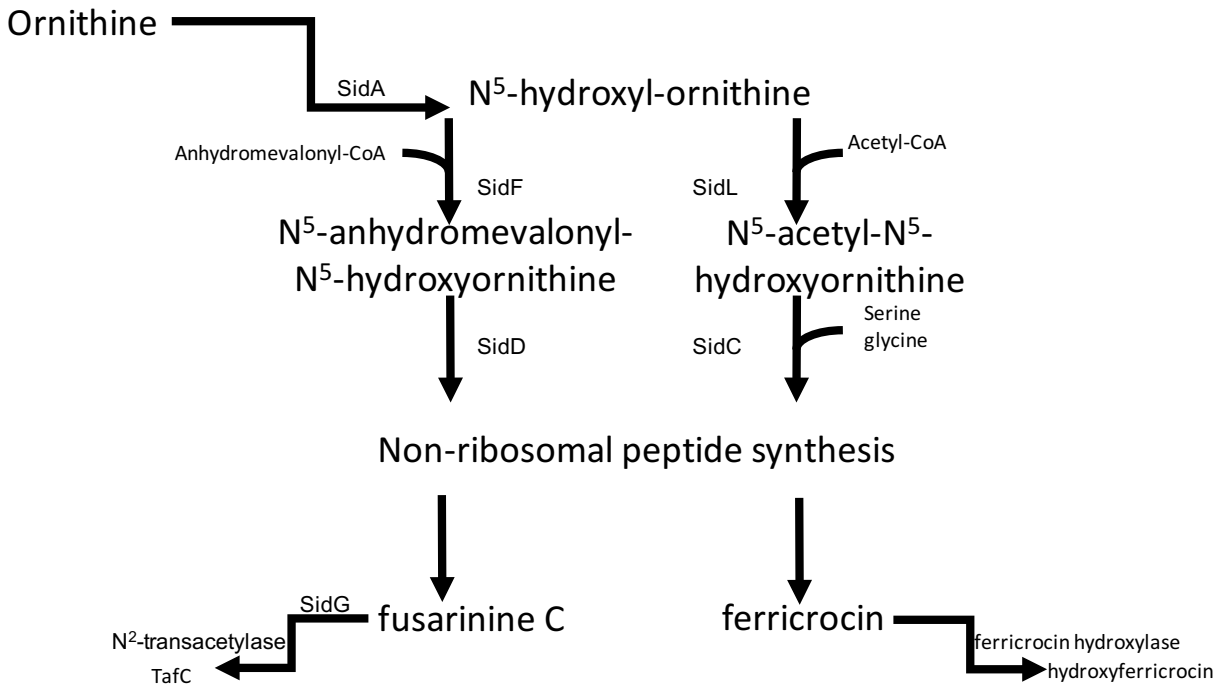

Figure 3: Siderophore biosynthetic pathway of *A. fumigatus* as described by Plattner and Diekmann(37). The biosynthesis of TAFC and FC starts with hydroxylation of L-ornithine leading to the formation of hydroxamate group by the transfer of an acyl group from acyl-coenzyme A (CoA). The pathway then splits to form the prefer acyl group for FC (acetyl) and TAFC (anhydromevalonyl). The cyclic siderophores assembly is catalyzed by non-ribosomal peptide synthetases. TAFC and hydroxyferricrocin by N^2-acetylation of fusarinine C and hydroxylation of FC respectively.

2.2 Materials and Methods

2.2.1 Materials

Buffers and media for bacterial growth were obtained from Fisher Scientific (Pittsburg, PA). *E. coli* Turbo BL21 (DE3) competent cells were purchased from Gelantis (San Diego, CA) and the pET-15b vector from Novagen. Protein purification was conducted on AKTA prime system (GE Healthcare) with 5 mL Ni-columns (GE Healthcare). NADPH and $NADP^+$ were obtained from EMD Bioscience (Billerica, MA). Acquity ultra-performance liquid chromatography (UPLC) and C18 (2.1 x 10 mm) analytical columns were purchased from Waters. The Kinase Inhibitors and NIH Clinical Collection Library was obtained from Selleckchem (Houston, TX) and NIHCC respectively. For the screening 384-well clear bottom Greiner plates were used and samples were analyzed on the SpectraMax M5 microplate spectrophotometer (Molecular Devices, Sunnyvale, CA). Ebselen and wortmannin were purchased from Fischer Scientific. Ebselen analogs Indan and, 2-phenyl-2,3-dihydro-1,2-benzothiazol-3-one were purchased from Sigma Aldrich while, Tavaborole were purchased from Vitas-M laboratory (Champaign, IL) and 2-phenyl-2,3-dihydro-1H-isoindol-1-one and 2-phenyl-2,3-dihydro-1,3-benzothiazole were from Molport (Riga, LV). *Aspergillus fumigatus* strain 46555 was obtained from the American Type Culture Collection (ATCC) and 12-well Corning tissue culture flat bottom plates were purchased from Fischer Scientific.

2.2.2 Fluorescence Polarization

High-throughput screening of the kinase library was also performed using the ADP-TAMRA (tetramethyl rhodamine) and the FP assay designed for SidA(38). In this assay, 384 well plates were used and the reaction volume was 15 µL using 50 mM potassium phosphate pH 7.0. In the screening 30 nM of ADP-TAMRA with 2 µM of SidA (based on the Bradford assay) and 20 and 200 µM of library compounds was used in a final DMSO concentration of 2%. Fluorescence Polarization measurements were conducted at an excitation of 544 nm and emission at 584 nm with a wavelength cutoff of 570 nm. Anisotropy values were normalized to the negative control (ADP-TAMRA, SidA and DMSO).

2.2.3 Activity Assay

High throughput screening of the two libraries (kinase library 273 compounds and NIH library 701 compounds) with a total of 973 compounds was performed using a variation of the Csaky iodine assay modified for HTS(39,40) at the Virginia Tech Center for Drug Discovery Screening Lab. Standard assay conditions included : 2 μM SidA (based on Bradford assay), 500 μM L-Orn, 250 μM NADPH in a final reaction volume of 15 μL in 100 mM sodium phosphate (pH 7.5), reaction was allowed to proceed for 30 min at 25 °C. For the screening 20 and 200 μM of library compound was used in a final reaction mixture of 2 % DMSO with or without 0.1% Triton X-100. Reaction was quench with 63 μL of the iodine mix (0.2 N perchloric acid, 4% sodium acetate,0.4% sulfanilic acid and 0.01% iodine in 100% acetic acid), incubated at 25 °C for 15 min. Then, 10 μL of 0.1 N sodium thiosulfate and 10 μL of 0.6% naphthylamine were added followed by a 10-min incubation. The absorbance of 1-naphthylamine red was recorded at 562 nm. The amount of hydroxylornithine produced was quantified using a standard curve with hydroxylamine (0- 350 μM). Activity values were normalized to the values obtained from the positive control (SidA and L-Orn) and the negative control (SidA, L-Orn and NADPH) samples.

2.2.4 IC_{50} determination via a Product Formation Assay

Hits identified in the primary screening and Ebselen analogs were purchased from independent vendors. Inhibitory activity was validated by determination of the amount of substrate and product with an Ultra performance liquid chromatography (UPLC) method described previously(41,42). The amount of hydroxylated L-Orn was also quantified using the colorimetric assay described above (41,42). For UPLC assays, SidA (2 μM) was incubated in a final reaction mixture of 10% DMSO with 250 μM NADPH, 500 μM L-Orn and inhibitors concentrations range from 0-1000 μM in 100 μL 50 mM Tris-HCl, pH 8.0, for 30 min. The reaction was quenched with 200 μL of 100 % acetonitrile and centrifuged at 13,000 rpm for 1 min. Next, 130 μL of the supernatant was removed and mixed with 25 μL of 200 mM borate, pH 8.0. The substrate and hydroxylated product was derivatized by the addition of 3.4 μL of 150 mM fluorenylmethyloxycarbonyl chloride (FMOC-Cl) with a 5-min incubation at RT. Excess FMOC-Cl was removed by adding 158 μL of 53 mM 1-aminoadamantane with a 15-min incubation at RT. Samples were analyzed by reverse phase UPLC on a C18 column by loading 5 μL of samples. The column was equilibrated in 60% eluent A (0.1% trifluoroacetic acid in water) at a flow rate of

0.5 mL/min. The samples eluted on linear gradient with eluent B (0.1% trifluoroacetic acid in acetonitrile) from 40 to 100 % in and monitored at 263 nm over a 10-min time.

2.2.5 ThermoFAD Assay

ThermoFAD assay consisted of 20 µL of 3 mg/mL of SidA, 2% DMSO in 50 mM Potassium Phosphate buffer pH 7.0(43). By measuring FAD fluorescence as a function of temperature with a heat ramp from 20-90 °C in 1 °C increments the melting temperature of SidA was determined. As reference DMSO was used and as positive control T_m was calculated with L-Orn (20 mM) and $NADP^+$ (2 mM). Ebselen and Wortmannin was added at concentration ranges between 0.1- 1000 µM. Measurements were made using an excitation wavelength range between 470 and 500 nm and a SYBR Green fluorescence emission filter of 523-543 nm.

2.2.6 NADPH Oxidation

To validated if the identified compounds (ebselen, wortmannin and 2-phenyl-2,3-dihydro-benzothazol-3-one) caused inhibition an NADPH oxidation experiment was performed in the absence of the substrate. Ebselen and Wortmannin (0-100 µM) was mixed with 2 µM SidA, 60 µM NADPH in 200 µL of 100 mM sodium phosphate buffer pH 7.5 with a final concentration of 10% DMSO. The negative control included 60 µM NADPH, 2 µM SidA in final DMSO concentration of 10% while the positive control included only 60 µM NADPH. The oxidation was monitored in a spectrophotometric assay by observing the decrease in absorbance of NADPH at 340 nm over 10 minutes.

2.2.7 Oxygen Consumption Assay

Oxygen consumption was monitored in 1 mL reactions with 100 mM Sodium phosphate pH 7.5 with varying substrates NADPH (0.05 -2 mM) and L-Orn (0.25- 10 mM) using a Hansatech Oxygraph (Norfolk, UK). Assay that included variation of NADPH, 10 mM L-Orn was held constant, 2 µM SidA in 100 mM sodium phosphate with 0, 2 and 11 µM Ebselen. In assays where L-Orn was varied, NADPH was held constant at 1 mM with 2 µM SidA in 100 mM sodium phosphate with 0, 2, 11 and 20 µM ebselen. Assays were initiated with NADPH and monitored under constant stirring.

2.2.8 Growth Inhibition

A. fumigatus (ATCC 46645) spores were germinated in potatoes dextrose agar (PDA) at 37 ºC. Then, spores were harvested using a sterile scraper from 3 day old cultures and suspended in phosphate saline buffer containing 0.1% Tween-20. For inhibition assays, *A. fumigatus* was grown on PDA, Aspergillus minimal medium (AMM-Fe), AMM containing 1.5 mM $FeCl_3$ (AMM+Fe), and blood agar (AMM-Fe containing 5% (v/v) sheep blood) (44,45). Inhibition of growth was tested using 12-well tissue culture plates containing 1.5 mL of agar and DMSO at a final concentration of 0.5% DMSO. DMSO and 27 μM amphotericin B were used as positive and negative control respectively. DMSO, Ebselen, Wortmannin or amphotericin B were mixed in with agar before solidifying. After 12 h at 4 ºC, wells were spot inoculated with 1 μL of 5 x 10^5 spores/mL and incubated at 37 °C. Growth was monitored every 6 h until 30 h were reached.

2.2.9 Data Analysis

The enzyme activity and anisotropy values in the primary screenings were normalized to the negative control sample (equation 1) where $\mu_{N,}$ $\mu_{20/200}$ and $\mu_{B\ represents}$ the mean value of the negative control, the compounds at 20 or 200 μM or background respectively. The Z- factor values were determined using equation 2 where $\sigma_{N,P}$ and $\mu_{N,P}$ represents the standard deviation and the mean value of the negative and positive controls respectively(46). The IC_{50} of compounds from the activity assay and UPLC was determined with a 10-point dose response curve and residual enzyme activity was fitted to equation 3 using Kaleidagraph. In equation 3 the parameters include the minimum or maximum values of the anisotropy or enzymatic activity as well as the x-value of mid-point of Y also known as the IC50. The m^{IC50} describes the slope of the curve at the midpoint value.

$$\%\ Activity = 100 * \frac{(1-(\mu_N - x))}{|\mu_N - \mu_{20/200}|} \qquad \text{Equation 1}$$

$$\%\ Anisotropy = 100 * \frac{(1-(\mu_{20/200} - x))}{|\mu_{20/200} - \mu_B|} \qquad \text{Equation 1.2}$$

$$Z - factor = 1 - \frac{3(\sigma_{P+\sigma_N})}{|\mu_{P-}\ \mu_N|} \qquad \text{Equation 2}$$

$$Y = min + \frac{(max-min)\times(x^{IC50})}{m^{IC50}+x^{IC50}} \qquad \text{Equation 3}$$

2.3 Results

2.3.1 Kinase Library Primary Screening

To identify compounds that could inhibit the activity of SidA, two different libraries were screened in a High-throughput format. The first library used was The Selleckchem Kinase. This library was composed of 273 structurally diverse inhibitors that targets aurora kinase, receptor tyrosine kinase and phosphoinositide 3-kinase and are competitive inhibitors against ATP. It was chosen because ATP and NADPH share structural similarities, both contain an adenine base and phosphate groups (Figure 4). These similarities are important since flavin-dependent monooxygenase have a NADPH binding pocket. In order to, anticipate the outcome of the kinase library on the screening against SidA, the effect that ATP has on SidA binding was analyzed using the hydroxylation activity assay. It was found that ATP binding is weak with an observe IC_{50} of 464 μM (Figure 4B). SidA was HTS against 20 and 200 μM compound concentration using a fluorescence polarization binding and enzymatic activity assay. The screening with the enzymatic assays was performed with 0.1% (v/v) Triton-X-100 to remove compounds whose mechanism of inhibition is through protein aggregation. In Figure 5A, the results from the primary screening using the fluorescence polarization assay can be seen. This assay uses the chromophore ADP-TAMRA (38). From the fluorescence polarization assay an overall Z- factor of 0.56 ±0.01 was observed for the experiment at compound concentration of 20 and 200 μM (2% DMSO). The Z-factor is a parameter that describes the separation between the positive and negative control. An acceptable Z-factor lies between 0.5 and 1 (46). The negative control for this assay include SidA, ADP-TAMRA and DMSO while the positive control was composed of ADP-TAMRA and DMSO.

In addition to the FP assay, inhibition of SidA activity using a colorimetric assay was also used. The colorimetric assay can result in three different type of outcomes. The first being a negative (100% enzyme activity) where a pink color is developed to indicate product (L-OH-Orn) formation. The second and third ones being no color development indicating no product formation (0 % enzyme activity) or a false positive (color quenching by chemical mechanism) respectively. False positives could be caused by two factors interference with assay (color quenching) or aggregation (protein denaturation). In this assay, there was an overall Z- factor of 0.97 ± 0.01 (Figure 5 B and C).

A

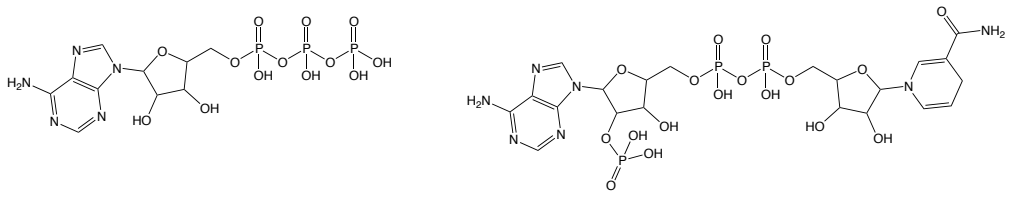

B

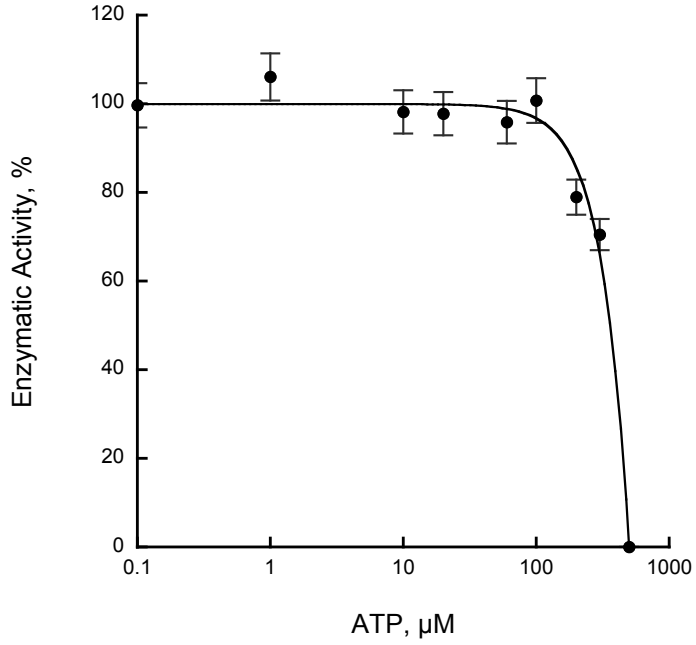

Figure 4: Chemical structure of (A). ATP and NADPH. (B). Inhibition of SidA enzymatic Activity by ATP in 10% DMSO determined by the hydroxylation activity assay. Reaction conditions: 2 μM of SidA, 500 μM L-Orn and 250 μM NADPH and 30 min reaction

2.3.2 NIH Library Primary Screening

The second library screened was the NIH collection library. This library is composed of 701 compounds that are diverse in function. Many the drugs found in this library are currently under clinical trials for treatment of a variety of diseases such as bipolar disorders, cancer and cardiovascular. This library was screened only with the colorimetric activity assay in the same HTS format as the kinase library in the presence of 0.1 % Triton-X-100. The Z-factor of 0.674 ± 0.002 observed for this library was also found in the acceptable range (Figure 7).

2.3.3 Identification and Validation of Hits

To distinguish between positive and false positive hits from the primary screening different factors were taken into consideration: 1) concentration effect in the presence and absences of detergent, 2) aggregation and 3) potency of inhibitor. In the case of the kinase library hits were first defined as compounds that demonstrated an anisotropy value in the HTS assay less than 60 % (normalized anisotropy) and showed to have a concentration effect at 20 and 200 μM. This resulted in nine hits, when parameters that affect enzymatic activity was added to the selection, only one compound was left triciribine phosphate. Since the fluorescence polarization assay shows more of binding than a quantitative way to detect inhibition of SidA enzymatic activity results were not further studied and a new hit definition was developed using the colorimetric activity assay (Table 2). The limits for defining Hits such as enzyme inhibition of 40 % was based on the value obtained three standard deviation below the mean for the assay mean. The same processed was used in identifying Hits from the NIH library. In the primary screening of the NIH library 3 compounds were identified as Hits: pindolol, ebselen and mesalamine.

Out of the 973 compounds screen 8 were identified as hits from the primary screening of both libraries (Table 3). Inhibitory action of the selected hits was first confirmed with the colorimetric activity assay before validation with RP-UPLC assay after purchased from different manufacture. It was found that 6 of these compounds were false positives due to factors such as interference in color development, lack of inhibitory activity, oxidized NADPH, or precipitation. The 2 compounds: ebselen and wortmannin were further studied.

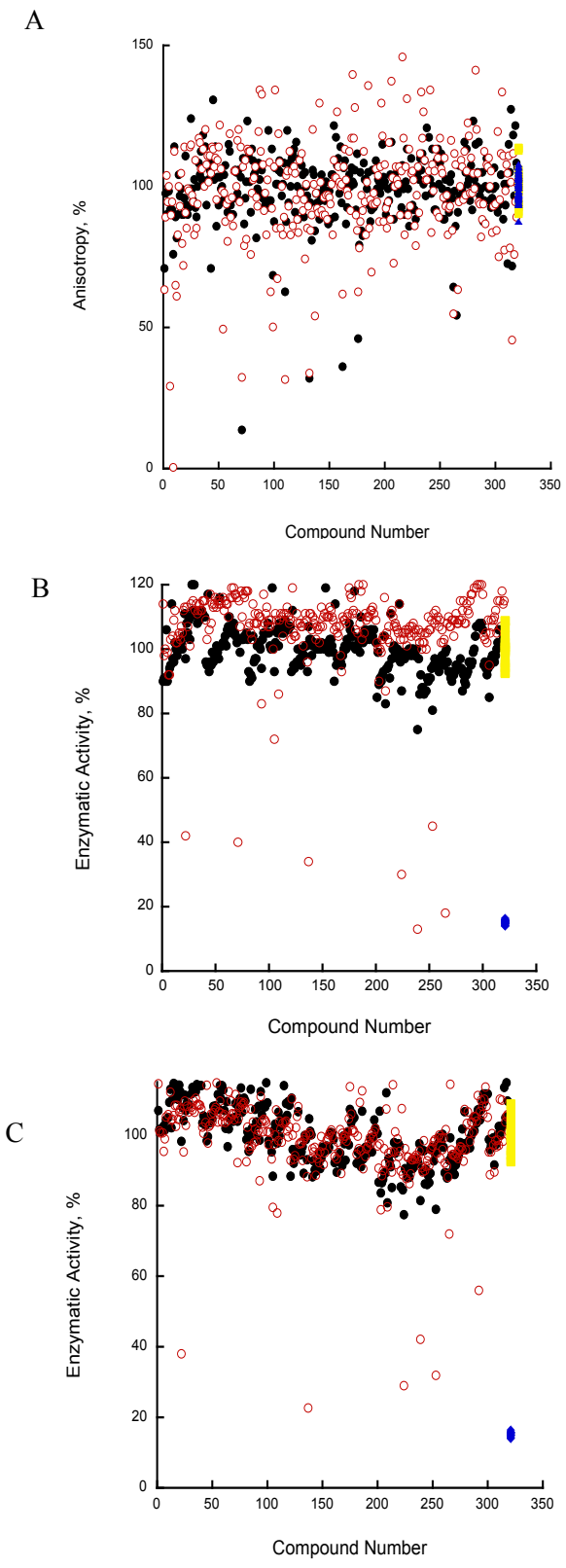

Figure 5: HTS of Kinase library against SidA via *(A)* FP assay and Colorimetric activity assay with (B) 0 % Triton-X-100 (C) 0.1% Triton-X-100. Compounds were evaluated as inhibitors by monitoring SidA enzymatic activity at 20 µM (●) and 200 µM (○) positive control (▲) and negative control (■).

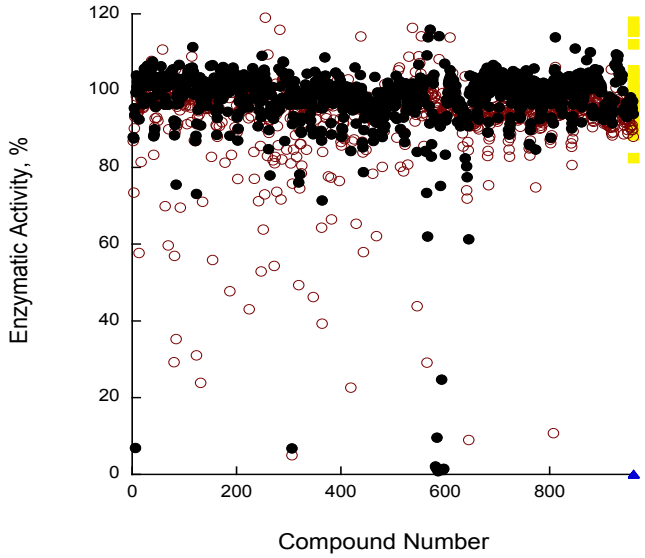

Figure 6: SidA Enzymatic Activity with 0.1% Triton-X-100 using NIH Library. Compounds were evaluated as potential inhibitors by monitoring SidA enzymatic activity at 20 µM (●) and 200 µM (○) positive control (▲) and negative control (■).

Table 2: Hit definition for kinase and NIH Library.

Hit Definition: Kinase and NIH Library
Enzyme Activity at 200 µM compound < 60
Enzyme Activity at 200 µM compound < 20 µM compound
Enzyme Activity at 200 µM compound with 0.1% Triton-X-100 < 60
Enzyme Activity at 200 µM compound with 0.1% Triton-X-100 < at 200 µM compound with 0.1% Triton-X-100
The difference between enzyme activity at 200 µM with and without 0.1 % Triton-X-100 < 30
The difference between enzyme activity at 20 µM with and without 0.1 % Triton-X-100 < 30

Table *3*: Summary of Compounds identified from new Hit Definition.

Compound Name	Structure
U0126-EtOH	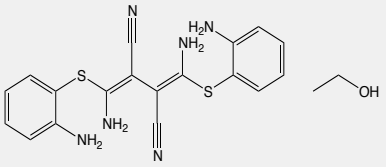
Arry-380	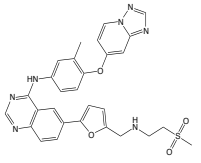
Wortmannin	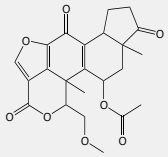
WP1066	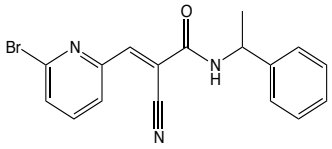
Triciribine Phosphate	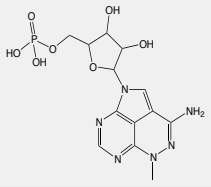
Ebselen	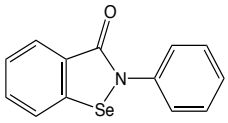
Pindolol	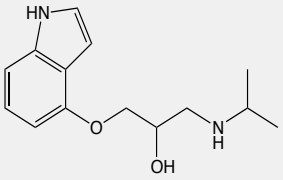
Mesalamine	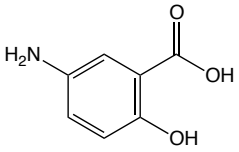

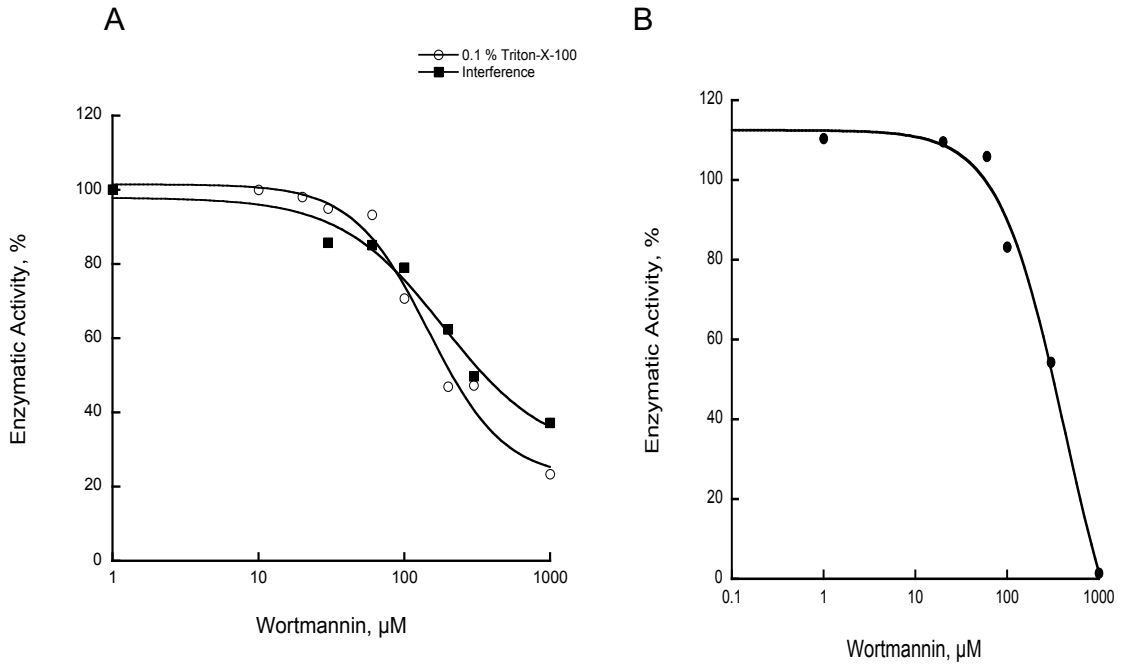

Figure 7: Inhibition of SidA enzymatic Activity by wortmannin (A). Hydroxylated activity assay with final DMSO concentration of 10%. (B). Product formation assay using RP- UPLC. Enzymatic reaction conditions included: 2 µM of SidA, 500 µM L-Orn, 250 µM NADPH and wortmannin (0-1000 µM).

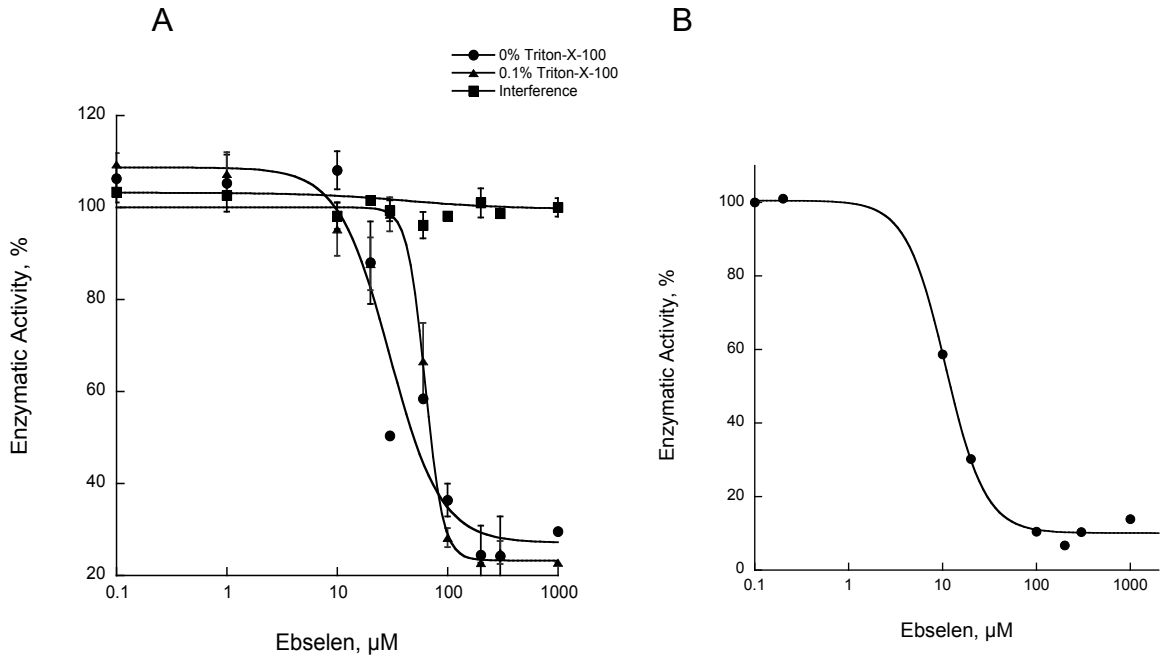

Figure 8: Inhibition of SidA enzymatic Activity by ebselen in (A). Hydroxylated activity assay with final DMSO concentration of 10%. (B). Product formation assay using RP- UPLC. Enzymatic reaction conditions included: 2 µM of SidA, 500 µM L-Orn, 250 µM NADPH and ebselen (0-1000 µM).

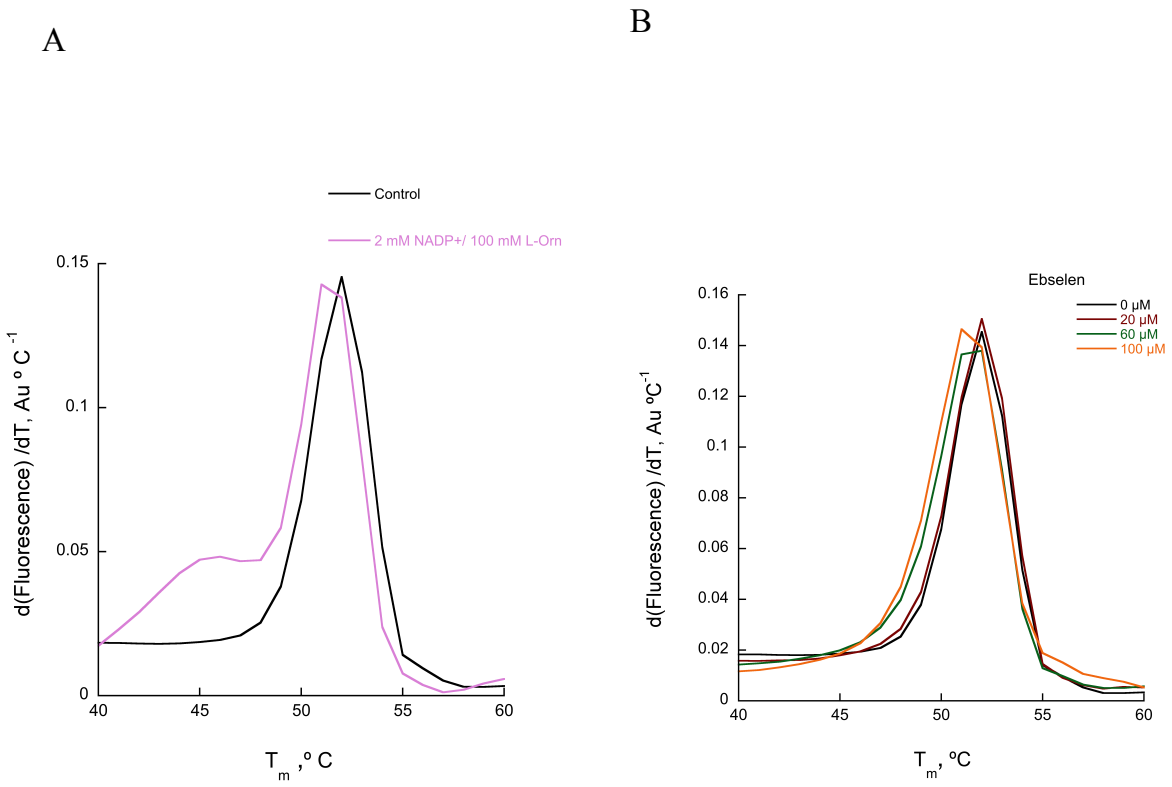

Figure 9: SidA Melting Curve obtaining via ThermoFAD assay. FAD was used as a fluorescence probe. (A). Saturating concentration of NADP $^{+}$ and L-Orn did not change melting temperature with control as reference. (B). Melting Curve of SidA with different ebselen concentrations, ebselen does not induced changes in melting temperature.

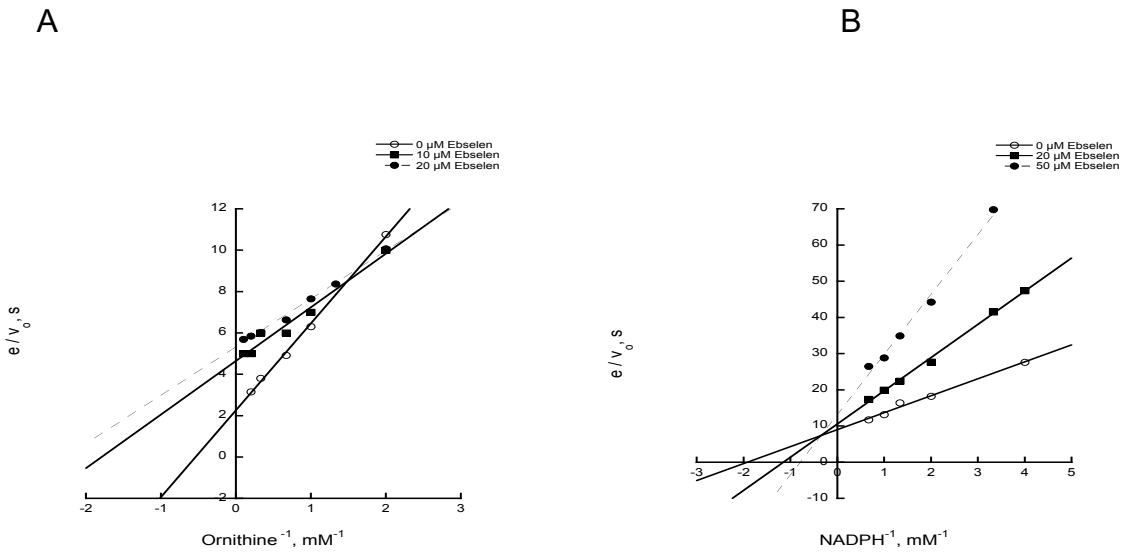

Figure 10: Double-reciprocal plot of varying ebselen concentrations in the presence of varying concentrations of (a) L-Orn (NADPH kept constant at 1 mM) and (b) NADPH (L-Orn kept constant at 10 mM).

2.3.4 Inhibition Studies

The IC_{50} of wortmannin and ebselen in 10 % DMSO was determined with a 10- point dosage curve using a colorimetric activity assay and verified with RP-UPLC product formation assay. Wortmannin, a phosphoinositide 3-kinase inhibitor, has shown to inhibit transcytosis in polarized epithelial cells (47). Wortmannin had a relatively weak binding affinity to SidA (IC_{50} 423 ± 286 μM, UPLC assay) and was not further studied (Figure 7).

An $IC_{50\ value}$ of 11 ± 1 μM was observed for ebselen via product formation assay using RP-UPLC (Figure 8). Ebselen was analyzed to determine if it was a denaturant of SidA. ThermoFAD studies were performed with 2 % DMSO and ebselen concentrations at 0-200 μM. Results showed that in the absence of the ligand the melting temperature was 48 °C and no substantial changes was observed in the presence of L-Orn and $NADP^+$. There was no changed observed in the T_m in the presence of ebselen at 0-60 μM. After 60 μM there is an increase in the T_m by 1°C (Figure 9).

The type of inhibition of ebselen was determined by measuring the amount of oxygen consumed by SidA as a function of ebselen, NADPH and L-Orn. Ebselen was validated as a non-competitive inhibitor for NADPH and L-Orn.

To assess if this inhibition occurred in a non-covalent mechanism, SidA was incubated with ebselen at concentrations 10-100 μM. Following a 15-min incubation the protein was diluted 25-fold and the reaction was initiated with L-Orn and NADPH. The potency of the compound at 10 -100 μM was the same as the DMSO control, confirming that Ebselen bind to SidA non-covalently (Figure 11).

A. fumigatus was grown in rich media (PDA) and in a minimum media with and without supplemented iron (AMM+Fe (III) and AMM-Fe Fe (III)) and in blood agar in the presence of ebselen (10-100 μM) with 0.5 % DMSO to examine in *cellulo* effect or the growth *of A. fumigatus*. Ebselen showed no inhibition of growth in the PDA medium indicating no toxicity against *A. fumigatus.* Also, no effect under the tested iron limiting conditions was observed. In the non-inoculated blood medium, ebselen did not caused hemolysis, abolishing the possibility of medium degradation that could lead from a minimum to a rich medium.

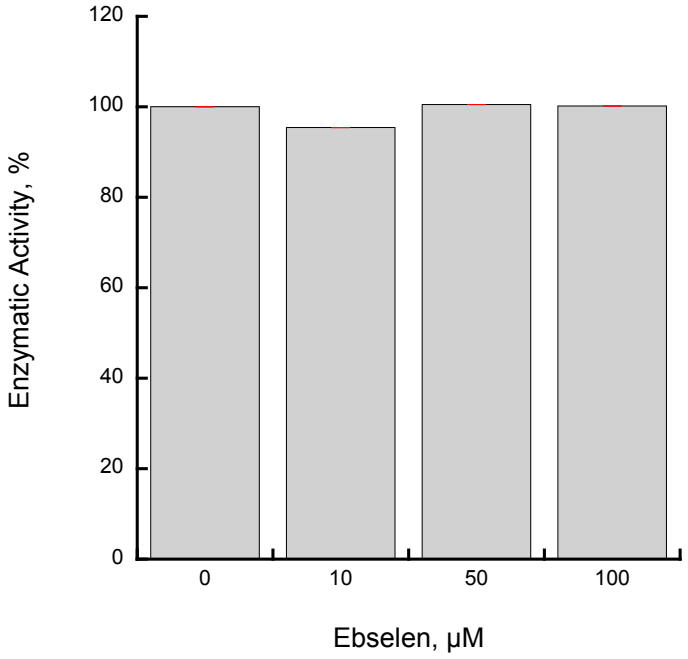

Figure 11: A comparison between the inhibition of SidA enzymatic with and without a 25-fold dilution of enzyme. The final 50 µL reaction contained 250 µM of L-Orn, 500 µM NADPH, ebselen (10-100 µM) and 35 µM SidA and 100 mM sodium phosphate buffer (pH 7.5)

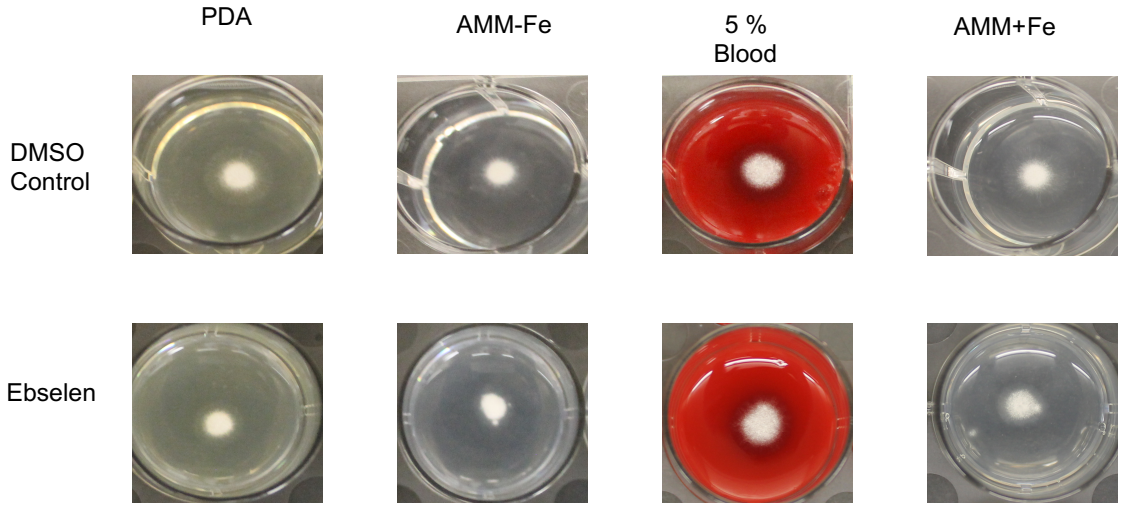

Figure 12: Ebselen effect on the growth of *A. fumigatus*. Pictures links to 24 h of incubation at 37 °C. *A. fumigatus* growth in different media supplemented with 50 µM ebselen. Media with AMM+Fe is complemented with 1.5 mM $FeCl_3$.

The non-inoculated blood medium ensured that the Fe-limiting condition was established and that siderophore assisted Fe-intake was the only Fe-acquisition system. This result confirmed the inability of ebselen to cause an in cellulo effect (Figure 12).

Six ebselen analogs were also tested using the colorimetric and RP-UPLC product formation assay. The analogs consist of compounds: patulin, indan, 2-phenyl-2,3-dihydro-1H-isoindol-1-one, 2-phenyl-2,3-dihydro-1,2-benzothiazol-3-one, tavaborole and 2-phenyl-2,3-dihydro-1,3-benzothiazole (Table 4). They all showed no inhibition of SidA except for 2-phenyl-2,3-dihydro-1,2-benzothiazol-3-one (ebsulfur) an IC_{50} of 40 ± 13 μM was observed from the product formation assay using RP-UPLC (Figure 13).

To validate inhibition of SidA enzymatic activity an NADPH oxidation assay was performed. Results confirmed that ebsulfur does cause inhibition of SidA activity in the absence of substrate (Figure 14). To verify that ebsulfur is not a SidA denaturant ThermoFAD studies were conducted. Experiments were performed at concentrations of 0-100 μM with 2 % DMSO. In the absence of the ligand the melting temperature was 48 °C and no changes were observed in the presence of L-Orn and $NADP^+$ as seen with ebselen studies. However, in the presence of ebsulfur there was an increase in the T_m by approximately 1°C (Figure 15).

The type of inhibition by ebsulfur was determined by measuring the activity of SidA as function of NADPH and ornithine at varying compound concentrations at 10% DMSO. Results shown as Lineweaver-Burk plots suggest that it is an uncompetitive inhibitor for NADPH and ornithine (Figure 16).

Table 4: Compound Name and Structure of ebselen Derivatives.

Compound Name	Structure
Patulin	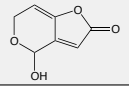
Indan	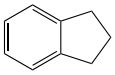
2-phenyl-2-3-dihydro-1H-isoindol-1-one	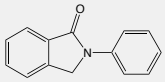
2-phenyl-2-3-dihydro-1,2-benzothiazol-3-one	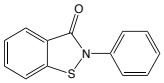
2-phenyl-2-3-dihydro-1,2-benzothiazole	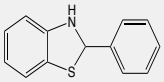
Tavaborole	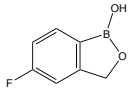

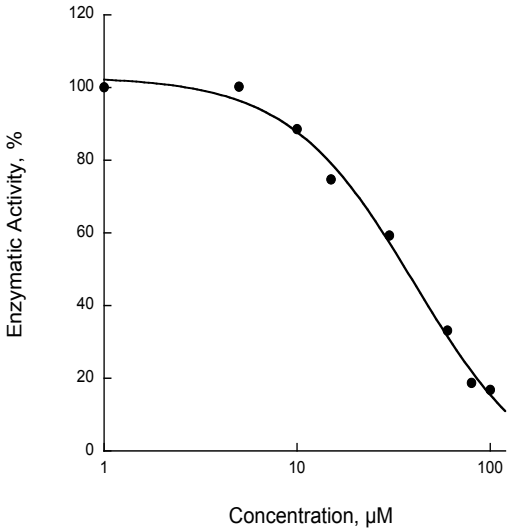

Figure 13: Ebsulfur dose response curve via RP-UPLC. Reaction conditions: 2 μM of SidA, 500 μM L-Orn and 250 μM NADPH.

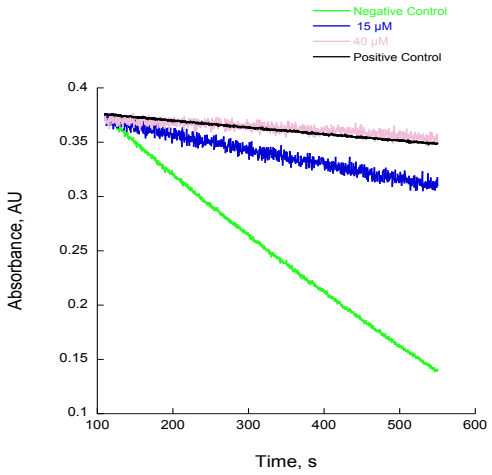

Figure 14: Time Course of NADPH Oxidation with Ebsulfur at 0- 100 µM and 2 µM SidA. Negative Control includes 60 µM NADPH, 2 µM SidA and 100 mM sodium phosphate pH 7.5. While Positive Control includes only 60 µM NADPH and buffer.

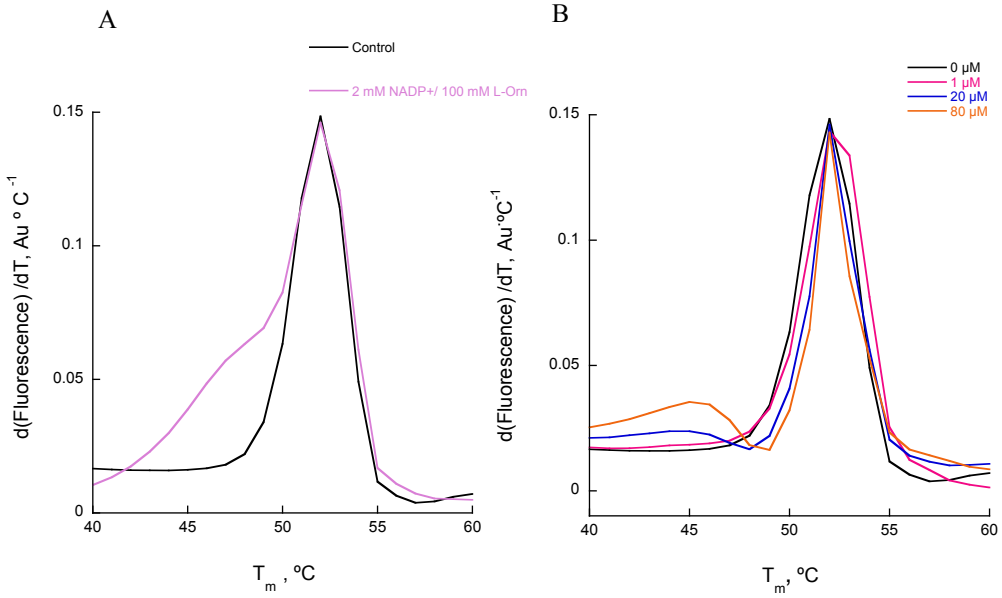

Figure 15: SidA Melting Curve obtaining via ThermoFAD assay. FAD was used as a fluorescence probe. (A). Saturating concentration of $NADP^+$ and L-Orn did not change melting temperature with control as reference. (B). Melting Curve of SidA with different Ebsulfur concentrations.

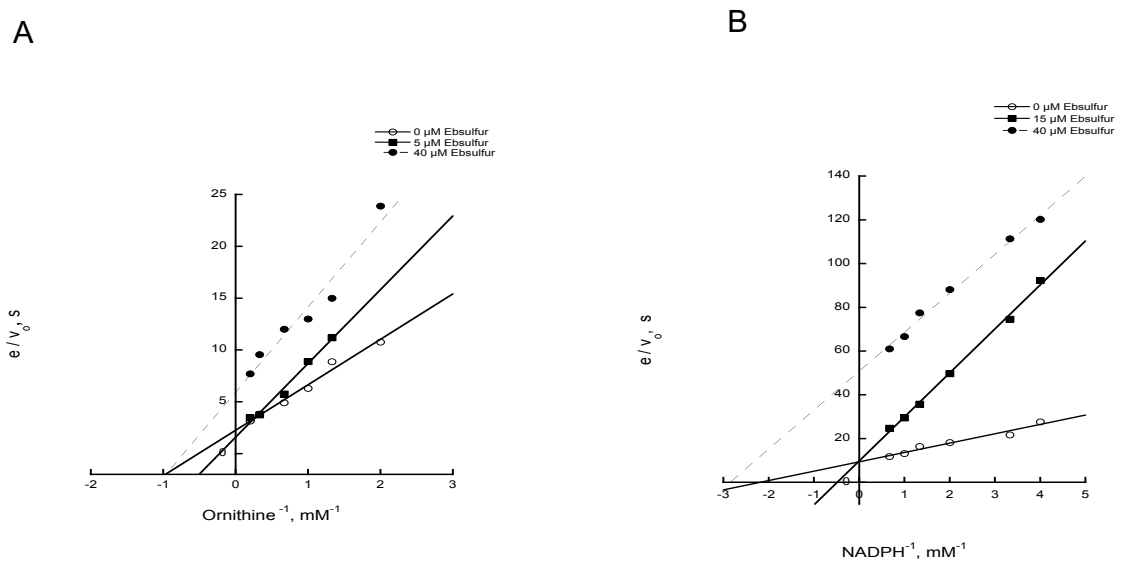

Figure 16: Double-reciprocal plot of varying Ebsulfur concentrations in the presence of varying concentrations of (a) L-Orn (NADPH kept constant at 1 mM) and (b) NADPH (L-Orn kept constant at 10 mM). The K_i values for L-Orn and NADPH are 6.2 ± 0.8 mM and 2.2 ± 0.5 mM respectively.

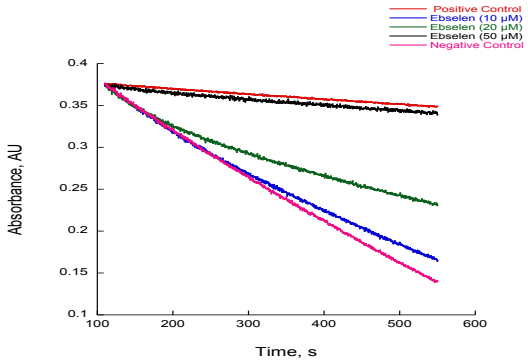

Figure 17: Time Course of NADPH (60 µM) Oxidation with ebselen at 0- 50 µM and 2 µM SidA. Negative Control includes 60 µM NADPH, 2 µM SidA and 100 mM sodium phosphate pH 7.5. While Positive Control includes only 60 µM NADPH and buffer.

2.4 Discussion

Although iron is an essential nutrient for the survival and bacteria and fungi there is limited availability of iron. By acquiring iron through siderophores during infections, bacteria and fungi circumvent the iron limitation imposed by the enhanced immunity response of the host (48). It has been confirmed that siderophore biosynthesis is essential for infection in bacteria and fungi. The increase in the drug resistance case has led to the need in the development and identification of new antifungal drugs (44). Many reports suggested that targeting iron acquisition systems is a promising drug target for fungal infections. This work has identified ebselen and ebsulfur as inhibitor of SidA by using previously reported screening methodology for identifying small molecules that can target siderophore biosynthesis in pathogenic fungi.

In SidA, ebselen demonstrates inhibition via a non-covalent interaction confirmed via a dilution assay. NADPH oxidation experiments confirmed ebselen inhibits SidA in the absence of the substrate (Figure 17). Inhibition of this reaction suggest that ebselen is preventing NADPH from binding via a non-competitive mechanism or inducing a conformational change altering the NADPH binding pocket of SidA. Ebselen mechanism of inhibition is not stimulate by destabilization of SidA verify by ThermoFAD assays. The results validate that ebselen as a non-competitive inhibitor against SidA that demonstrates an IC_{50} of 11 μM.

Commercially available analogs of ebselen was purchased and analyzed to determine the chemical group responsible for inhibiting SidA activity. Modifications include removing of a phenyl group and replacement of ketone group with amine. With these substitutions SidA activity was not inhibited. This suggested that the phenyl group and ketone at position 2 and 3 of ebselen was required for inhibition of SidA activity. Other modifications were also made in which selenium was replaced with a nitrogen or carbon atom while other functional groups remain the same. No inhibition was observed with the modification with carbon however, the change with sulfur lead to the identification of a new inhibitor 2-phenyl-2,3-dihydro-1,2-benzothiazol-3-one referred to as ebsulfur.

Ebsulfur showed a 4-fold higher IC_{50} than ebselen suggesting that the selenium atom is playing an active role in the inhibition of SidA activity. It was expected that ebsulfur would show some type of inhibition because of the similarities in sulfur and selenium chemical properties. Sulfur is located directly above selenium in the periodic table and both can adopts similar oxidation states -2, +4 or + 6 making them capable of multiple bonding (49). Further improvements in

ebselen and ebsulfur inhibition of SidA can possibly assisted in the identification or development of a new generation of antifungal compounds.

Chapter 3: *Amycolatopsis alba* monooxygenase

3.1 Introduction

In 2015 it was reported that a new hydroxamate containing a siderophore named albachelin (Figure 18) was isolated from a culture of *Amycolatopsis alba*(50) grown under iron deficient conditions. The structure of albachelin consist of six molecules of amino acids including: one molecule of N-α-acethyl-N-δ-hydroxy-N-δ-formylornithine, N-α-methyl-N-δ-hydroxyornithine and cyclic N-hydroxyornithine respectively and three molecules of serine. Similar to *A. fumigatus*, the siderophore pathway in *Amycolatopsis alba* encodes for a L-ornithine monooxygenase referred from now on as AMO. Sequence alignment shows the amino acid sequences of SidA and AMO are 31% identical, yielding a structural model with high similarity (Figure 19). This chapter focuses on the expression, purification, and pre-steady/steady-state characterization of the unique single-component enzyme *AMO*. Pre-steady state characterization will focus on monitoring the reductive- half reaction of AMO. While steady state characterization of AMO will give insight into oxygen consumption, N^5–hydroxyl-L-ornithine production and hydrogen peroxide formation. These aims will enable us to better understand the NMO class of flavoenzymes and their mechanism of action.

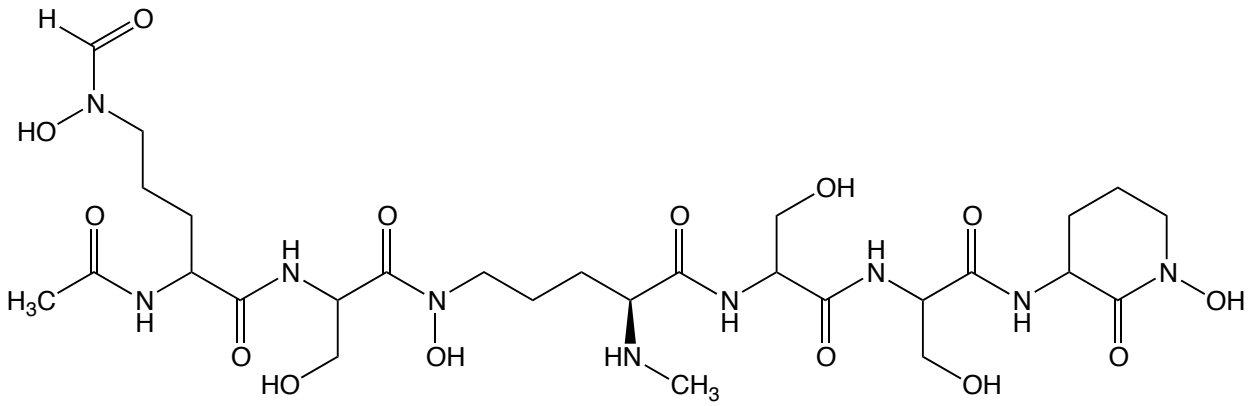

Figure 18: A chemical structure of desferri-albachelin.

A

```
SidA MESVERKSESSYLGMRNMQPEQRLSLDPPRLRSTPQDELHDLLCVGFGPASLAIAIALHD
AMO  ---------------------------MARAVFGERVPVYDVVGVGFGPSNLALAIAVTE

SidA ALDPRLNKSASNIHAQPKICFLERQKQFAWHSGMLVPGSKMQISFIKDLATLRDPRSSFT
AMO  HNAAPGAETVT-------AHFLERQACFGWHRGMLIDNATMQVSFLKDLATMRNPTSSFS

SidA FLNYLHQKGRLIHFTNLSTFLPARLEFEDYMRWCAQQFSDVVAYGEEVVEVIPGKSDPSS
AMO  FLSYLHSKDRLVDFINHKNLFPLRIEFHDYFEWAAEKVDDLVSYGTEVLSVTPVFD---G

SidA SVVDFFTVRSRNVETGEISARRTRKVVIAIGGTAKMPSGLPQDPRIIHSSKYCTTLPALL
AMO  DEIEFFDVHAR--TDGELVNLRARNLVMGTGLRPNLPEGVTPGTRVWHNSELLHRVEGMA

SidA KDKSKPYNIAVLGSGQSAAEIFHDLQKRYPNSRTTLIMRDSAMRPSDDSPFVNEIFNPER
AMO  AE--EPRRFVVVGAGQSAAEVSALLHDRFPQAEVCAVFARYGYSPADDSAFANRIFDPEA

SidA VDKFYSQSAAERQRSLLADKATNYSVVRLELIEEIYNDMYLQRVKNPDETQWQHRILPER
AMO  VGRFYEAPEAVKDRLMRYHGATNYSAVDIDLIDELYRRVYREKVQGVER----LRLINVS

SidA KITRVEHHGPQSRMRIHLKSSKPESEGAANDVKETLEVDALMVATGYNRNAHERLLSKVQ
AMO  RPTEVVDTGSEVRVTVEALES---------GERTRIDADFVVYATGYSPADPTSLLGELA

SidA HLRPTGQD-QWKPHRDYRVEMDPSKVSSEAGIWLQGCNERTHGLSDSLLSVLAVRGGEMV
AMO  SACARDDEGRLRVERDYRIVTEP---PLDGGIYLQGGTEHTHGITSSLLSNTAVRVGEIL

SidA QSIFGEQLERAAVQGHQLRAML--
AMO  QSIVDRRVADASRPEYAVSGTGPA
```

B

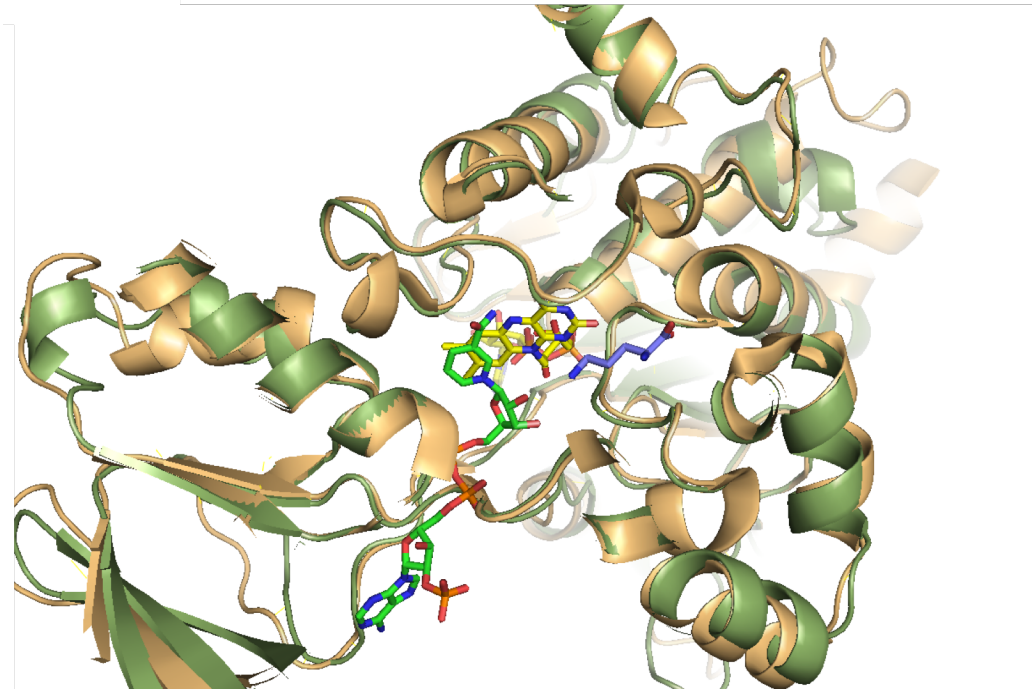

Figure 19. (A) Sequence alignment of AMO and SidA performed with Biology workbench. Gaps represented with dash, conserved residues in green (B) Structure alignment of AfSidA (PDB 4B63, cyan) and phyre (51) model of AMO (wheat). FAD is shown as stick in color yellow and $NADP^+$ is shown in green.

3.2.1 Materials

E. coli Turbo Bl21 (DE3) chemically competent cells were purchased from Invitrogen. Purification was performed on an AKTA Start FPLC (GE Healthcare). L-Orn, L-Lys, buffers, salts, kanamycin and NADPH, NADH, 96 well-plates, and pierce hydrogen peroxide detection kits were purchased from Thermo-Fisher Scientifics. Oxygen consumption systems were conducted on Hansatech Oxygraph (Norfolk, UK), while rapid-reaction studies were conducted on Applied Photophysics SX20 stopped-flow spectrophotometry (Leatherhead, UK) housed in Coy Glove box (Grass Lake, MI). Glucose oxidase was obtained from MP Biomedical (Solon, OH).

3.2.2 AMO Expression and Purification

Turbo BL21 (DE3) *Escherichia coli* cells containing the pVP56K AMO plasmid were plated onto Luria-Bertani broth (LB) plates supplemented with 100 μg/mL kanamycin. A single colony from the plates was used to inoculate two 50 mL LB medium flasks with 100 μg/mL of kanamycin. The culture was incubated overnight at 37 °C with continuous shaking at 250 rpm. Six 2.8 L Fernbach flasks each containing 1 L of Terrific Broth (TB) auto-induction medium(phosphate buffer, succinic acid, $MgSO_4$, and 30X media containing 15% (w/v) lactose, 24% (v/v) glycerol and 0.45% (w/v) glucose)(52,53) were inoculated with 8 mL of overnight culture and kept at 37 °C with agitation at 250 rpm until the optical density at 600 nm (OD_{600}) reached a value of approximately 5.0. Then, the temperature was reduced to 18 °C for 18 h. The cells were harvested by centrifugation at 4000 x *g* for twenty min. The resulting cell paste (~ 65g) were stored at -80 °C until purification.

Frozen cell pellets were resuspended in 200 mL of buffer A (25 mM HEPES buffer, pH 7.5 containing 300 mM NaCl and 25 mM Imidazole) with 1 mM phenylmethanesulfonylfluroide, 150 µM FAD and 50 µg/mL of lysozyme and 25 µg/mL DNase and RNase each. The resuspended cells were mixed for 15 min at 4 °C then sonicated (Fischer Scientific Sonic Dismembrator Model 500) at 70 % amplitude for fifteen minutes with a pulse of 5 s on and 10 s off in an ice bath. The lysate was centrifuged at 34500 g for an 1 h to remove cell debris.

The resulting supernatant was then loaded onto three-in-tandem 5 mL HisTrap FF crude columns (GE Healthcare) previously pre-equilibrated with buffer A at a flow rate of 5 mL/min. After loading, the column was washed with buffer A, and bound recombinant AMO was eluted

with 100% buffer B (25 mM HEPES buffer, pH 7.5 with 300 mM NaCl, and 300 mM Imidazole) using 300 mM imidazole at a flow rate of 2 mL/min. After purification, fractions containing AMO were pooled and dialyzed overnight at 4 °C in buffer C (25 mM HEPES buffer, pH 7.5 containing 300 mM NaCl and 10% glycerol) containing 10 μg/mL TEV protease for MBP cleavage. The final imidazole concentration after dialyzed was less than 1 mM. The next day, the protein was removed from the dialysis bag and loaded at 2.5 mL/min onto 3 in tandem 5 mL His Trap FF crude columns equilibrated with buffers C. The holoenzyme form of AMO eluted at 1 mM imidazole the apo-AMO eluted at 9 mM imidazole. Fractions containing AMO (based on SDS-PAGE) were pooled, then diluted with storage buffer (25 mM HEPES pH 7.5, 150 mM NaCl, 10% Glycerol) and concentrated using a 30 kDa Amicon ® Ultra Centrifugal filter membrane (Billerica, MA). Protein concentration was quantified using the Bradford Assay (MW 49 kDa) and the calculated extinction coefficient (ε 450 = 12,000 $M^{-1}cm^{-1}$) for holo-AMO. Aliquots were frozen in liquid nitrogen in approximately 20 μL beads prior to storage at -80 °C.

3.2.3 Determination of the Bound Flavin Extinction Coefficient to Holo-AMO

The spectrum of purified AMO in 100 mM sodium phosphate pH 7.5 was recorded in a 1 cm pathlength quartz cuvette. After data collection, the sample was incubated at 95 °C for 10 min. The resulting solution was centrifuged for 5 min at 13.2 *g* in a bench centrifuge and the supernatant removed to record the UV-Vis spectra of the liberated FAD. An extinction coefficient at 450 nm of 12000 $M^{-1}\cdot cm^{-1}$ was calculated for the amount of FAD bound to AMO using the extinction coefficient of 11300 M^{-1} cm^{-1} for free FAD(54).

3.2.4 Gel Filtration Chromatography

AMO was loaded onto HiPrep Sephacryl S-200 HR, GE Healthcare column equilibrated with 50 mM potassium phosphate and 150 mM NaCl buffer at pH 7. As standards, Ferritin (440000), ribonuclease A (13700 Da), ovalbumin (43000 Da), conalbumin (75000 Da), aldolase (158000 Da) were used along with blue dextran200.

3.2.5 Oxygen Consumption Assay

Oxygen consumed by AMO was monitored using the Hansatech Oxygraph Plus System (Norfolk, VA) in 1 mL cell reaction. The standard assay buffer contains 100 mM sodium phosphate

buffer, pH 7.5. Assays were NADPH or NADH was varied L-Orn was held constant and 10 mM and NAD(P)H was constant at 5 mM for reactions where L-Lys or L-Orn was varied. The assay was initialed with 2.5 μM (holo-AMO) or 5 μM (apo-AMO) AMO. For the apo-AMO 15 μM of FAD was incorporated into the reaction for activation of the enzyme.

3.2.6 Hydroxylation Assay for Determination of N-hydroxylation

Using a variation of the Csaky iodine oxidation assay the amount of hydroxylated product formed by AMO was determined (39,55,56). The standard assay buffer was 100 mM sodium phosphate pH 7.5. The reaction was started by the addition of enzyme (10 μM for apo and 5 μM for holo) to 10 mM L-Orn or 1 mM NADPH in a reaction volume of 100 μL (15 μM of FAD was incorporated into the reaction for the apoenzyme. The reaction was incubated for 30 min before it was terminated by the addition of 50 μL of 0.2 N perchloric acid. After quenching the mixture was centrifuged for 1 min at 13.2 x *g* and then 50 μL of the were transferred to a clear- 96 well plate. The reaction mixture was neutralized by adding 47.5 μL of 10% (w/v) sodium acetate solution follow by 47.5 μL of 1% (w/v) sulfanilic acid in 25% (v/v) acetic acid. To each well 19 μL of 0.1 % (w/v) iodide in glacial acetic acid was added and the reaction was incubated at room temperature for 15 min. Then, 19 μL of 0.1 N sodium thiosulfate was used to remove the excess iodine from the solution. The color was developed by the addition of 19 μL of 0.6% (w/v) α -naphthylamine in 30% (v/v) acetic acid. The absorbance at 562 nm was measured after 15 min using a Spectra-Max M5 plate reader (Molecular Devices). The amount of hydroxylated product formed was determine using a hydroxylamine hydrochloride (0-300 μM) standard curve.

3.2.7 Detection of Hydrogen Peroxide Formation

Hydrogen peroxide was quantified using the Pierce hydrogen peroxide detection kit as previously described (40,57). The standard assay buffer was 100 mM sodium phosphate pH 7.5. The amount of hydrogen peroxide formed was determined as function of L-Orn and L-Lys (0-15 mM) and NADH and NADPH (0-6 mM) in 60 μL reaction. In assays where NADPH/NADH was varied, L-Orn was held constant at 10 mM and NAD(P)H was held constant at 1 mM in reactions where L-Orn was varied. Reactions were initiated with 10 μM of AMO and allowed to proceed at 25 ºC for 30 min with constant shaking at 750 rpm. Aliquots of 20 μL were then mixed with 200 μL working reagent composed of 100 mM sorbitol, 125 μM xyenol orange and 250 μM

ammonium ferrous(II) sulfate and 25 mM H_2SO_4 in water. The mixture was then incubated for 10 min at 25 °C and the absorbance was recorded at 595 nm. A hydrogen peroxide standard curve was used to quantified the amount of hydrogen peroxide produced by AMO.

3.2.8 Flavin Reduction in the Presence of L-Ornithine

Reduction of FAD bound to AMO was monitored at 15 °C in a single mode using stopped flow spectrometry (Applied Photophysics SX20, Leatherhead, UK) under anaerobic condition in the glove box. The reaction buffer consisted of 20 mM Tris-sulfate, 50 mM NaCl, pH 8.0 and was made anaerobically using methods previously reported(58). Reduction of FAD was monitored using the reductant NADPH and NADH in the presence of L-ornithine. The reaction mixture consisted of 10 mM L-ornithine, 10 μM or 50 μM of the holo or apo enzyme respectively and varied concentration of the reductant (0- 4 mM). 10 μM of FAD was incorporated into the reaction for the apo-AMO. Reduction of AMO was monitored with a photodiode array spectrometer until full reduction of FAD was achieved by the detection of decrease in absorbance at 450 nm. Measurements were recorded on a logarithmic scale in triplicates. The observed rate constants of NAD(P)H at various concentrations were determined using the program KaleidaGraph (Synergy software, Reading, PA) by fitting the data to a double exponential decay equation. The rate constants for the observed phases of the reaction was plotted against varying concentrations of NADPH/NADH and fitted to equation 3 to obtain the k_{red} and K_D of the reduction process.

3.2.9 Data Analysis

All kinetic data were fitted using the Kaleidagraph software to fit the Micahelis-Menten equation (Equation 1). For pre-steady state kinetics, the data was fitted to double exponential decay for reduction experiments (Equation 2). The resulting k_{obs} values were plotted as a function of NADPH or NADH concentrations using Equation 3 to obtain the rate of reduction k_{red} and K_D values.

$$v = \frac{V_{max}[S]}{K_M+[S]} \quad \text{(Eq.1)}$$

$$v = A_1 e^{-k_{obs1}t} + A_2 e^{-k_{obs2}t} + C \quad \text{(Eq. 2)}$$

$$k_{obs} = \frac{k_{red}[S]}{K_M+[S]} \quad \text{(Eq.3)}$$

Results

3.3.1 Expression and Purification of AMO

Recombinant AMO was expressed as a fusion to 8x-his-MBP in pVP56K (Figure 21). The incorporation of His_8 tag at the N-terminus of MBP allowed the use of immobilized affinity columns (IMAC). The purified fusion protein was cleaved from the His_8-MBP tag by the addition of tobacco etch virus (TEV) protease which has a recognition sequence between the C-terminus of MBP and N-terminus of AMO. After overnight cleavage, the protein solution was loaded onto two in-tandem 5 mL HisTrap columns. Holo-AMO was eluted in the mobile phase and apo-AMO eluted at 90 mM Imidazole (Figure 20B). Overall, a total of 120 mg of purified protein was obtained from 63 g of cell paste, yielded a 95 % purity per liter of culture. Figure 18 °C shows a spectrum of an FAD cofactor bound to the purified holoenzyme with a maxima absorbance observed at 380 and 450 nm (Figure 20C). This yielded a flavin incorporation of approximately 55- 70 % for holo-AMO. This was determined by dividing the protein concentration calculated using the flavin extinction coefficient (12000 M^{-1} cm^{-1}) by the protein concentration obtained by the Bradford assay.

The oligomeric state of holo-AMO and apo-AMO were determine using size exclusion chromatography. It was determined that holo-AMO and apo-AMO adopts different quaternary structures. Holo-AMO shows octamer and trimer characteristics, whereas apo-AMO adopts an octamer and tetramer structure. Apo-AMO was also run in the presence of FAD and in this case the oligomer state stayed the same a tetramer (Figure 21).

3.3.2 Enzyme Activity Varying Substrate Concentrations

The activity of AMO was monitored by measuring the rate of oxygen consumption with a constant concentration of NADPH (5 mM). Apo-AMO consumes oxygen with an apparent k_{cat} of 0.182 ± 0.01 s^{-1}. In comparison holo-AMO consumes oxygen with an k_{cat} of 0.342 ± 0.026 s^{-1}, this is 56 % higher than what was observed by apo-AMO. In contrast, when L-ornithine is the substrate the observed k_{cat} for apo-AMO in product formation is 20 times lower than the k_{cat} (0.010 ± 0.003 s^{-1}) determine using the oxygen consumption assay (Figure 22). While holo-AMO demonstrates an k_{cat} of 0.200 ± 0.006 s^{-1} using the product formation assay (Table 5).

Overall, apo-AMO is highly active in the presence of L-Orn having approximately a 2-fold higher activity based on K_{cat}/K_M with L-Orn than the holoenzyme with NADPH at 5 mM with the

oxygen consumption assay. This trend is also observed with L-Lys as the substrate for the apo-AMO and holo-AMO. Both apo-AMO and holo-AMO shows a higher affinity to L-Orn as the substrate in comparison to L-Lys by a 1.8-fold. There was no product observed with L-Lys as the substrate. It was determined by using the hydrogen peroxide assay that oxygen molecules are converted to hydrogen peroxide instead of product. An k_{cat} of 0.075 s^{-1} was observed for the apo-AMO compared to a value of 0.165 s^{-1} for the holo-AMO with L-Lys in the peroxide assay (Figure 23). These k_{cat} are similar to what was observed with L-Orn in the product formation assay

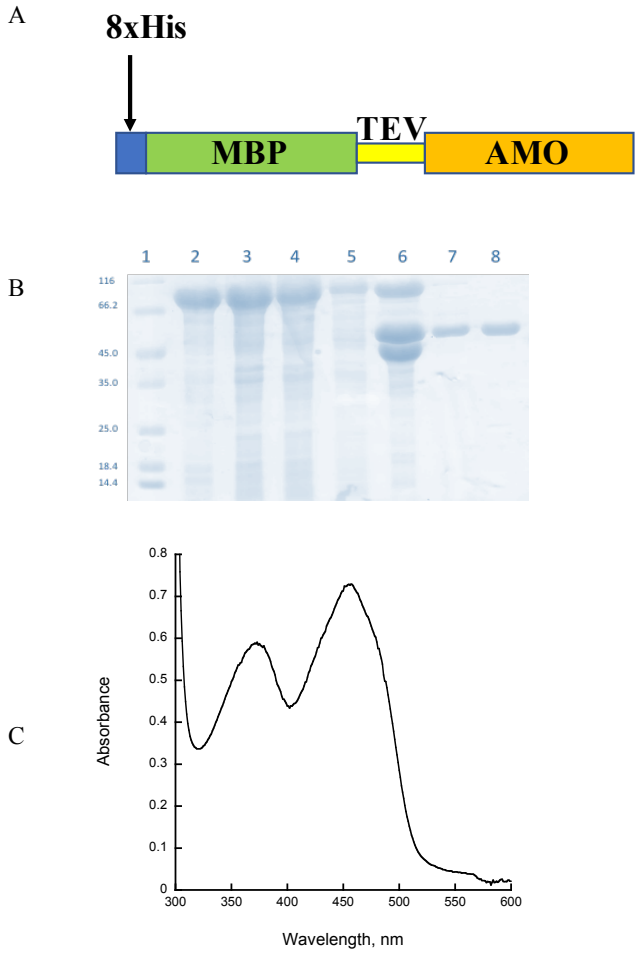

Figure 20: Summary of AMO purification. (A) Schematic of the pVP56K vector. (B) SDS-PAGE gel summarizing the purification of AMO: lane 1: molecular weight, lane 2: pellet, lane 3: soluble, lane 4: unbound, lane 5: wash, lane 6: sample from IMAC lane, 7: holo-AMO and lane 8: apo-AMO. (C). UV-visible spectrum of bound FAD in purified holo-AMO which has absorbance, λ maximum at 380 and 450 nm.

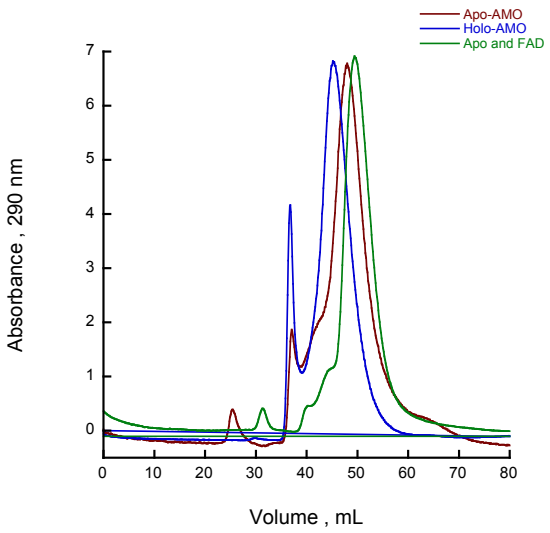

Figure 21: Size exclusion chromatography pattern in 50 mM potassium phosphate and 0.15 M NaCl buffer pH 7. (A) Holo-AMO (blue), Apo-AMO (purple) and Apo and FAD indicates apo-AMO in the presence of FAD inside the running buffer (green).

Table 5: Activity of AMO monitored by oxygen consumption (white box) and product formation (gray box) varying substrate concentrations. Conditions in 100 mM sodium phosphate buffer pH 7.5 in with 5 mM NADPH.

Parameters		Holo-AMO		Apo-AMO	
		L-Orn	L-Lys	L-Orn	L-Lys
k_{cat} (s^{-1})	Oxygraph	0.342 ± 0.026	0.342 ± 0.017	0.182 ± 0.012	0.168 ± 0.012
	Product formation	0.200 ± 0.006	N/A	0.010 ± 0.003	N/A
K_M (mM)	Oxygraph	0.305 ± 0.108	0.558 ± 0.108	0.107 ± 0.052	0.178 ± 0.073
	Product formation	0.234 ± 0.048	N/A	0.244 ± 0.035	N/A
K_{cat}/K_M (s^{-1}/mM)	Oxygraph	1121 ± 406	613 ± 122	1701 ± 834	944 ± 392
	Product formation	858 ± 178	N/A	43 ± 14	N/A

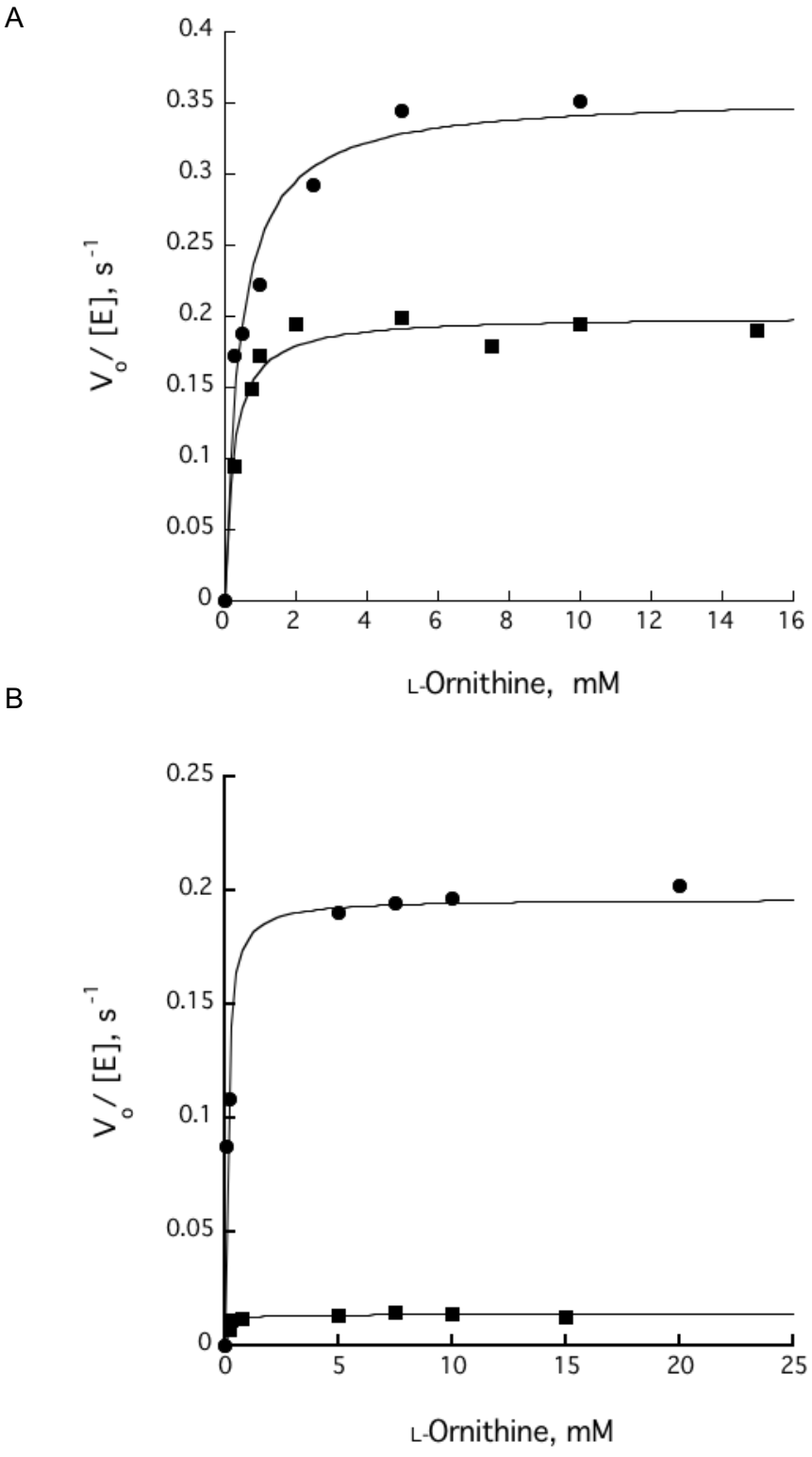

Figure 22: L-Orn saturation curves determine via oxygen consumptions and product formation assays. (A) holo-AMO and (B) apo-AMO saturation curve using oxygen consumption (●) and product formation (■).

A

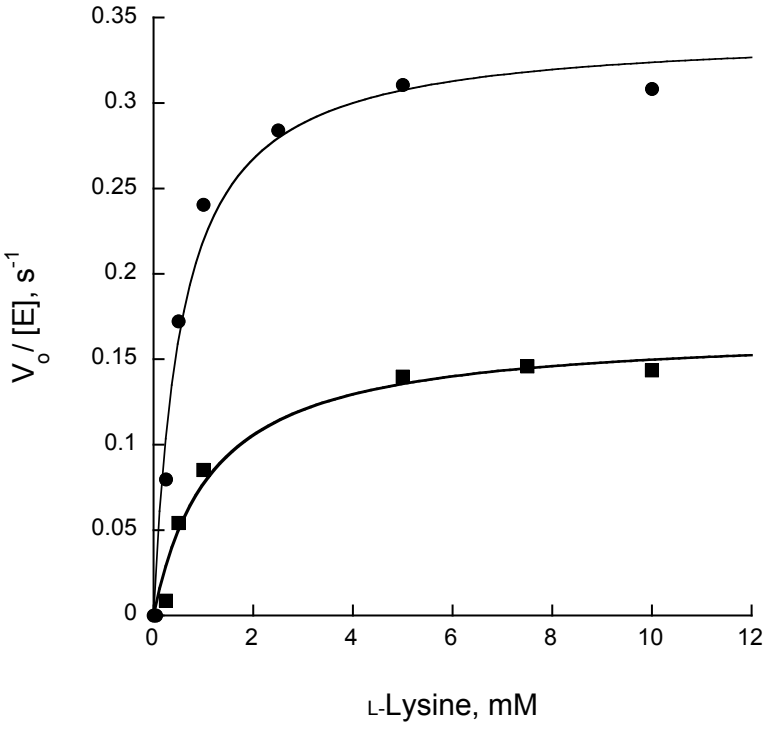

B

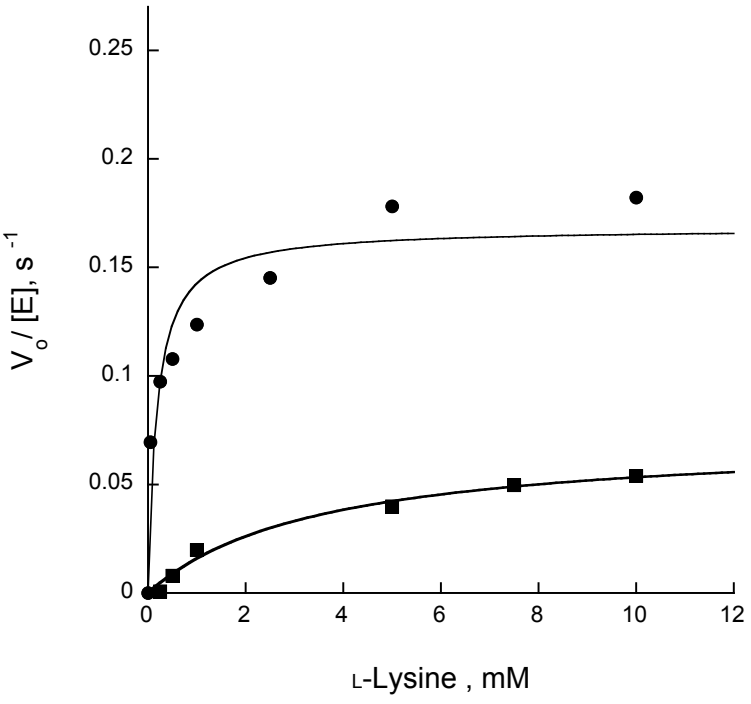

Figure 23: L-Lys saturation curves determine via oxygen consumptions and hydrogen peroxide. (A) holo- AMO (B). apo-AMO L-Lys saturation curve using oxygen consumption (●) and hydrogen peroxide (■).

3.3.3 Enzyme Activity Varying Reduced Nicotinamide Coenzyme Concentrations

By measuring the rate of oxygen consumption and product formation with ornithine at various NADPH concentrations, we found that, the k_{cat} was nearly identical for apo-AMO and holo-AMO (Table 6 and Figure 24). This trend is also seen when NADH is used as the coenzyme for apo-AMO with both assays. In the oxygen consumption assay, the observed k_{cat} for holo-AMO was 65 % higher for NADPH than NADH. However, for holo-AMO no product is formed when ornithine and NADH is used as the substrate and coenzyme (Figure 25). The preferred coenzyme for holo-AMO and apo-AMO was NADPH and NADH respectively determine by the lower K_M observed in the oxygen consumption and product formation assay.

3.3.4 Hydrogen Peroxide Formation

To detect if every oxygen molecule by AMO was channeled toward product formation the amount of hydrogen peroxide produced was quantified. Production of hydrogen peroxide as function of L-Orn or reduced nicotinamide coenzyme is shown in Figure 26. There is decrease in the amount of hydrogen peroxide produced ranging from 60 to 0 μM as the concentration of L-Orn increase in the presence of NADPH. This value is double the amount of peroxide produce by apo-AMO. In contrast, we observed an increase in reduced nicotinamide concentration hydrogen peroxide production increases as well. With NADPH hydrogen peroxide increases from 0 to 40 or 70 μM for the holo-AMO and apo-AMO respectively. Using NADH as the coenzyme apo-Holo produces a maximum of 120 μM of hydrogen peroxide to the 110 μM seen with holo-AMO. These results suggest that NADPH is the preferred coenzyme.

Table 6: Activity of AMO monitored by oxygen consumption (white box) and product formation (gray box) varying reduced nicotinamide coenzyme concentrations. *Conditions in 100 mM sodium phosphate buffer pH 7.5 in with 10 mM L-Orn.

Parameters		Holo-AMO		Apo-AMO	
		NADPH	NADH	NADPH	NADH
k_{cat} (s^{-1})	Oxygraph	0.232 ± 0.008	0.153 ± 0.011	0.170 ± 0.008	0.174 ± 0.009
	Product formation	0.077 ± 0.011	N/A	0.077 ± 0.066	0.04 ± 0.010
K_M (mM)	Oxygraph	1.400 ± 0.165	3.150 ± 0.086	2.740 ± 0.346	1.620 ± 0.230
	Product formation	0.64 ± 0.18	N/A	2.740 ± 2.92	0.561 ± 0.293
K_{cat}/K_M (s^{-1}/mM)	Oxygraph	163 ± 59	116 ± 9	62 ± 8	107 ± 15
	Product formation	120 ± 39	N/A	29 ± 40	71 ± 41

A

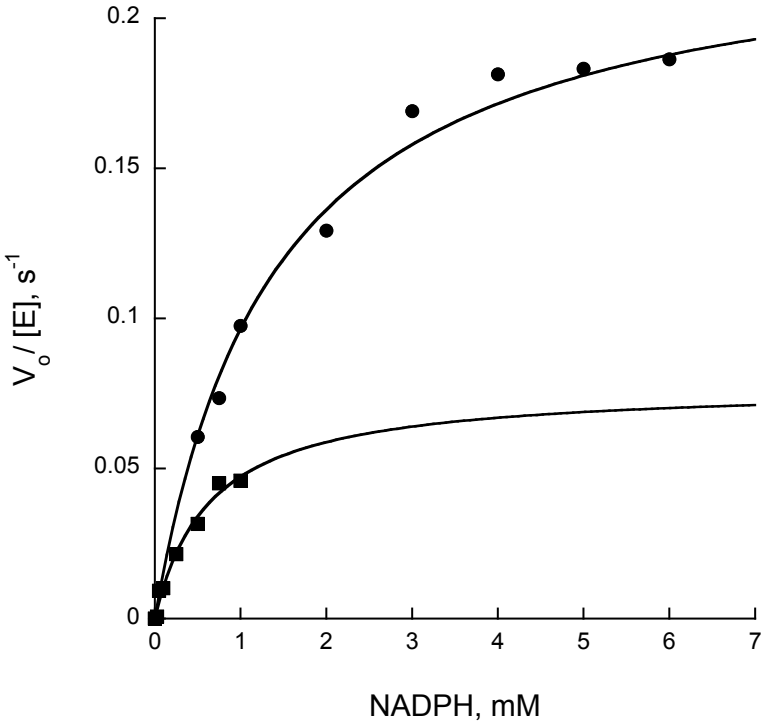

B

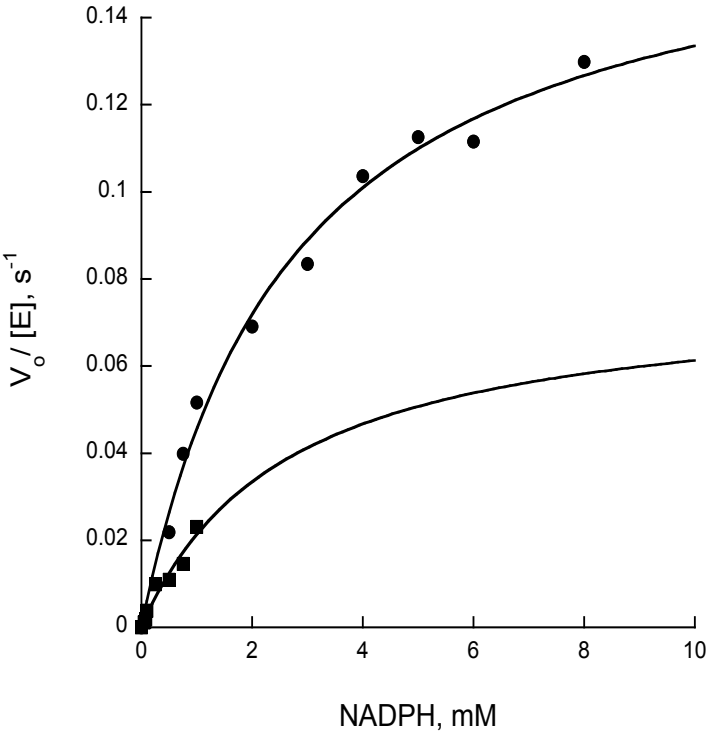

Figure 24: Reduced nicotinamide coenzyme saturation curves determine with NADPH. (A) holo AMO and (B) apo-AMO NADPH saturation curve using oxygen consumption (●) and product formation (■).

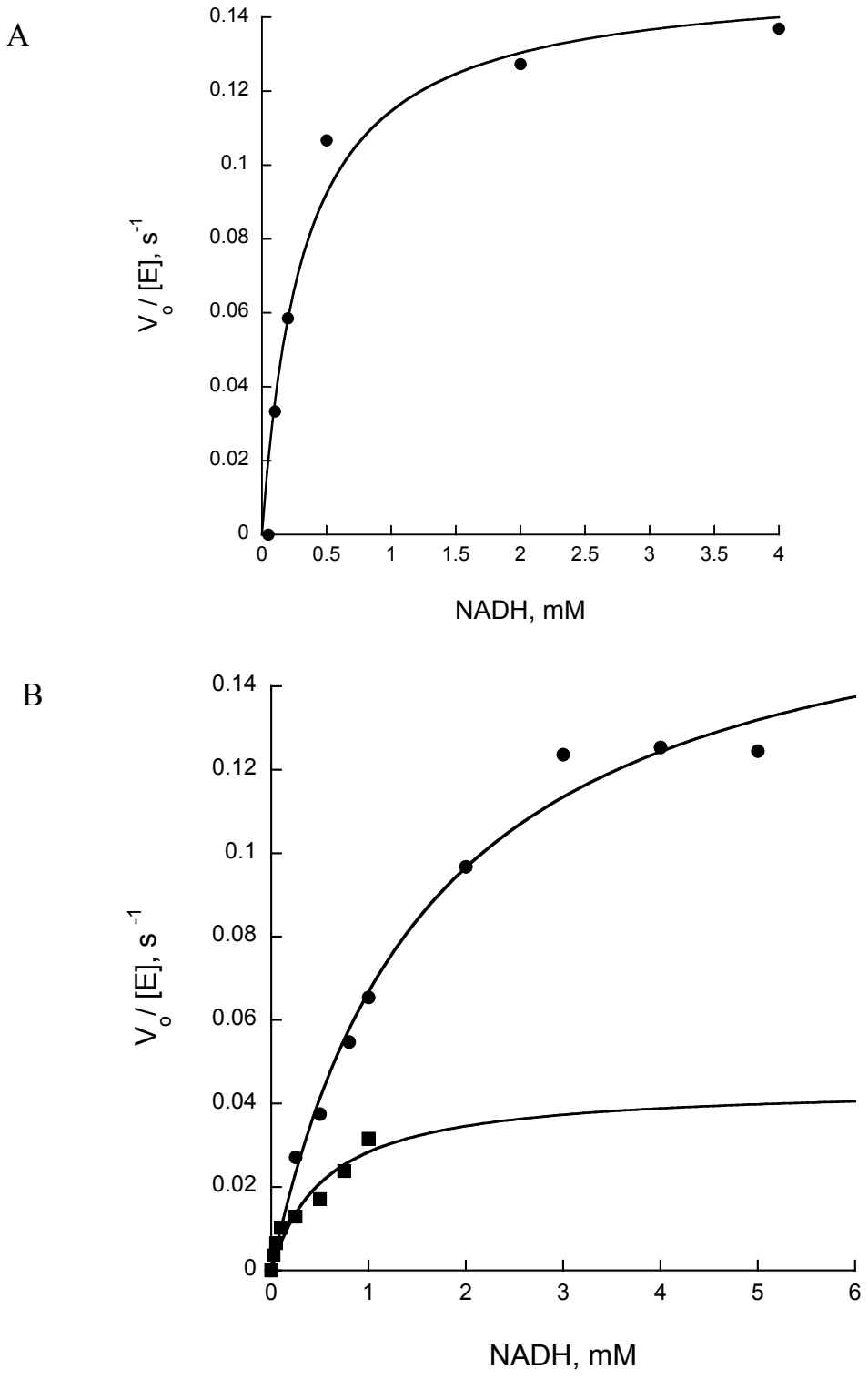

Figure 25: Reduced nicotinamide coenzyme saturation curves with NADH. (A) holo AMO and (B) apo-AMO saturation curve using oxygen consumption (●) and product formation (■).

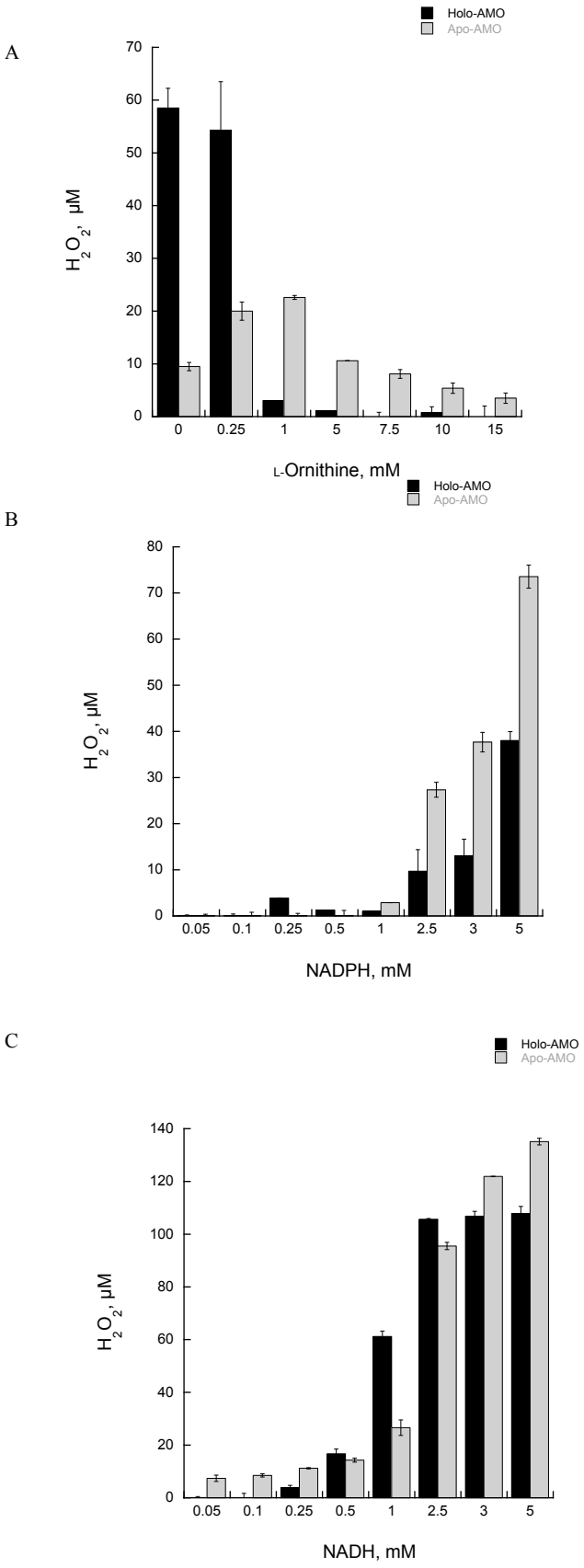

Figure 26: Hydrogen Peroxide Formation of AMO as function of (A) L-Orn in the presence of 1 mM NADPH, (B) NADPH and (C) NADH in the presence of 10 mM L-Orn.

3.3.5 Flavin Reduction in presence of L-Ornithine

Flavin reduction was monitored as a function of NAD(P)H in the presence of L-Orn. The reaction was monitored by measuring the decrease in absorbance at 450 nm in the stopped-flow spectrophotometer using a single-mixing mode. The reduction as observed in Figure 27A with holo-AMO and NADPH was relatively slow and was complete in 600 s at 100 μM NADPH. The reduction of FAD bound to holo-AMO follow a single-phase kinetics (Figure 27B) and dependent on NADPH concentration. The rate of reduction, k_{red} was calculated as 0.286 ± 0.031 s^{-1} and the K_D of holo-AMO for NADPH was 280 ± 94 μM. The catalytic efficiency k_{red}/K_D was 1021 $M^{-1}s^{-1}$ (Figure 27C).

The reduction of FAD with apo-AMO enzyme was also slow and was completed in 600 s at 100 μM NADPH (Figure 27 D and E). The rate of reduction, k_{red} was calculated as 0.198 ± 0.023 s^{-1} and the K_D of apo-AMO for NADPH was 1329 ± 370 μM. The catalytic efficiency k_{red}/K_D was 149 $M^{-1}s^{-1}$ (Figure 27 F). The data for calculating the reduction rates was determined based on equation 2.1 and 3. The double-fitting was used for both forms of AMO because it showed better fitting than the single.

The reduction kinetics of Flavin by NADH also occurred in one phase (Figure 28 A and D). Reduction rate k_{red} was calculated as 0.212 ± 0.010 s^{-1} and the K_D of holo-AMO was 420 ± 49 μM when NADH concentrations was varied. The catalytic efficiency k_{red}/K_D was 505 $M^{-1}s^{-1}$ (Figure 28 C). While for apo-AMO the rate of reduction, k_{red} was calculated as 0.219 ± 0.006 s^{-1} and the K_D of holo-AMO for NADH was 85 ± 15 μM. The catalytic efficiency k_{red}/K_D was 2576 $M^{-1}s^{-1}$ (Figure 28 F). Overall, the results indicate the preferred coenzyme for holo-AMO and apo-AMO was NADPH and NADH respectively which is consistent with the steady-state kinetics data (Table 7).

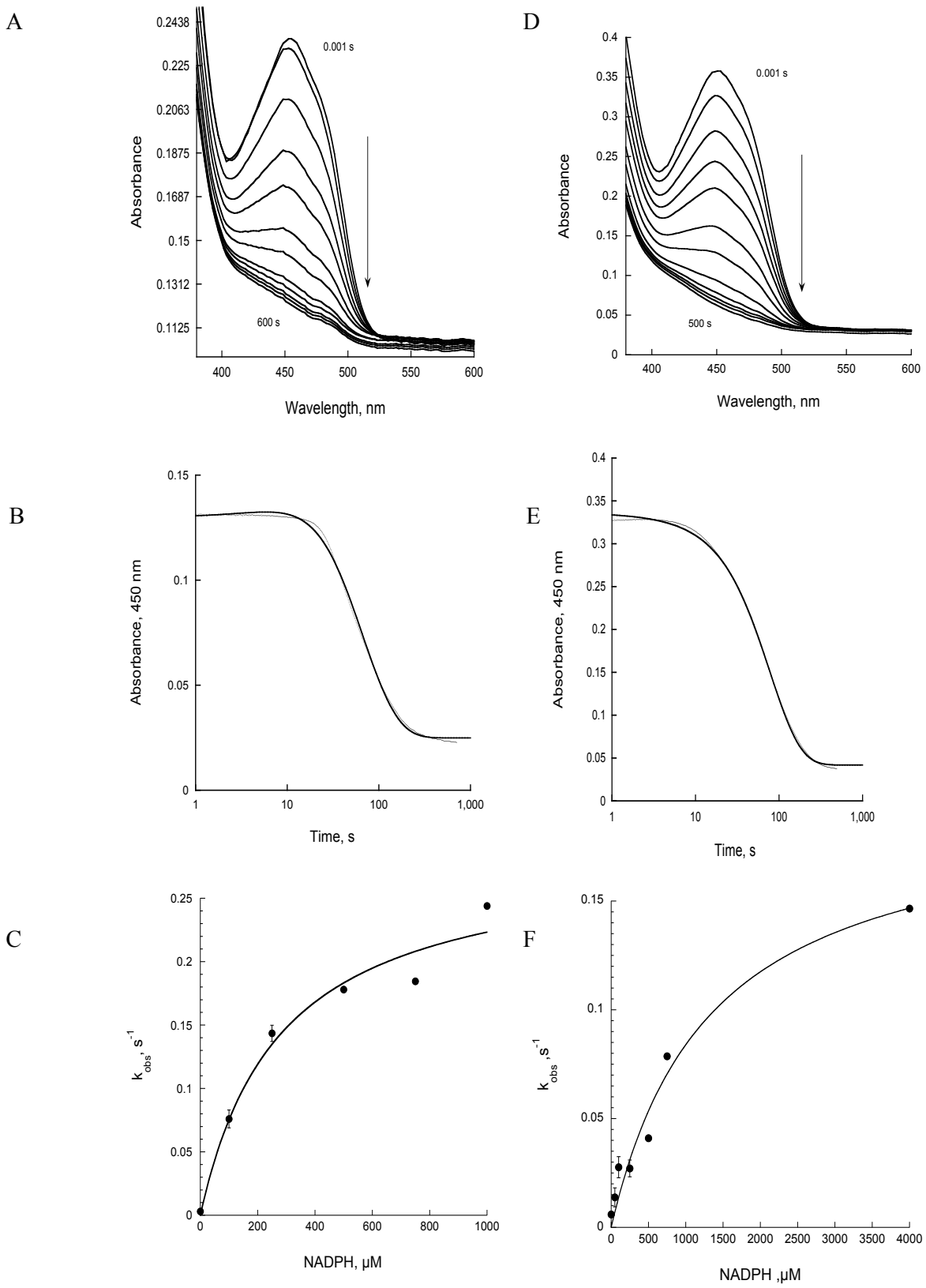

Figure 27: Flavin Reduction with holo-AMO and apo-AMO using NADPH. (A) spectra of reduction with 100 μM NADPH monitored over 600 s. (B) Changes in the flavin absorbance at 452 nm at 100 μM NADPH. The changes at absorbance at 450 nm were fit to Equation 2 to obtain the k_{obs} values. (C) Flavin Reduction using NADPH. The apparent k_{obs} values measured at each concentration of NADPH and plot as a function of NADPH concentrations (0-1000 μM). Panel D-F same as A-C respectively just with Apo-AMO instead.

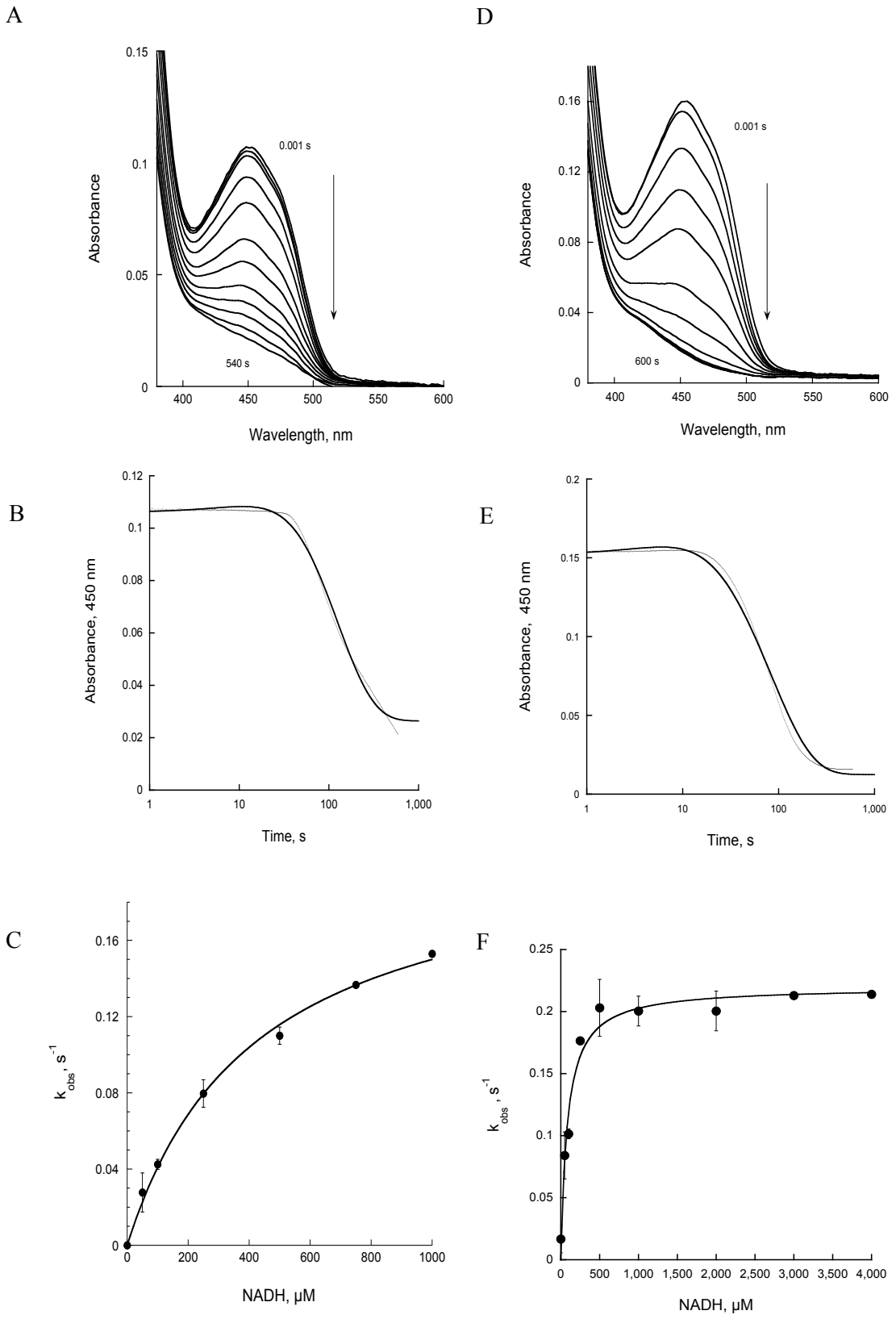

Figure 28: Flavin Reduction with holo-AMO and apo-AMO using NADH. (A) spectra of reduction with 100 µM NADH monitored over 540 s. (B) Changes in the flavin absorbance at 452 nm at 100 µM NADH. The changes at absorbance at 450 nm were fit to Equation 2 to obtain the k_{obs} values. (C) Flavin Reduction using NADH. The apparent *kobs* values measured at each concentration of NADH and plot as a function of NADH concentrations (0-1000 µM). Panel D-F same as A-C respectively just with Apo-AMO instead.

Table 7: Rapid reaction kinetic parameters for Flavin reductase activity
*Conditions were 20 mM Tris-Sulfate, 50 mM NaCl pH 8.0 at 15 ºC.

Parameters	Holo-AMO		Apo-AMO	
	NADPH	NADH	NADPH	NADH
k_{red} (s^{-1})	0.286 ± 0.031	0.198 ± 0.023	0.212 ± 0.010	0.219 ± 0.006
K_D (µM)	280 ± 94	1329 ± 370	420 ± 49	85 ± 15
k_{red}/K_D ($M\ s^{-1}$)	1021 ± 360	149 ± 45	505 ± 64	2576 ± 456

3.4 Discussion

NMOs are known to hydroxylate the amino groups of L-lysine and L-ornithine which leads to the formation of hydroxamate in the iron-binding site of siderophores. This thesis reports the characterization of AMO, an N^5-ornithine hydroxylase from *A. alba*. AMO is closely related to the L-ornithine N-hydroxylase from *Kutzneria* sp. 744 (KtzI). They share a 48 % sequence similarity and both hydroxylate the primary amine of L-ornithine side chain. KtzI is known to produce kutznerides a class of hexadepsipeptides that have both antimicrobial and antifungal properties(59). Similar to AMO, enzymatic activity of KtzI is dependent on FAD as the flavin cofactor although NADPH or NADH can be used as the source for the reducing equivalents. One difference between AMO and related Class B monooxygenase such as KtzI and SidA is that it can be purified with and without bound flavin cofactor.

Various mechanism of actions of flavin monooxygenases has been determined. For PvdA(60) , PHBH(11) and SidA(20) , members of the single-component enzymes , mechanisms are regulated by the order of addition of the substrate and product release (Scheme 1). For instance, PvdA does not require the binding of the substrate to be hydroxylated for reduction of flavin to occur. The reduction of the half-reaction is equally facile in the presence or absence of L-ornithine. Flavin reduction requires NADPH and then binds to molecular oxygen for formation of the peroxyflavin intermediate. This intermediate reacts with the oxidized substrate to form water and the hydroxylated product(60). On the other hand, for reduction of FAD in PHBH, a class A flavin monooxygenase, the substrate must be bound for reduction to occur by NADPH. This step is

follow by the release of $NADP^+$ and binding of molecular oxygen. The reduced flavin is capable of reoxidizing quickly by forming two intermediates before the formation of product, water and oxidized flavin.

However, AMO seems to follow a different mechanism than SidA in the reduction of flavin. In SidA reduction occurs in two steps; the first phase occurs at a much faster rate than the second and is concentration dependent(38). The rate in the second phase is not dependent on coenzyme concentration. It can be concluded from our data that AMO reduction follows a monophasic pattern and occurs at a very slow rate for both holo and apo-AMO. Data gathered in this study show AMO could be reduced in the absence of L-ornithine, suggesting that maybe the substrate does not bind to the oxidized from of the enzyme. In the presence of L-ornithine there is not substantial changes in the rate of flavin reduction indicating the flavin reduction is independent of substrate.

In some aspect AMO does not function as other flavin-dependent monooxygenases. Here, I show that the kinetics parameters for AMO which is 24-fold lower than what is reported for SidA in product formation. It is seen that k_{cat} values are lower with apo-AMO in the presence of L-ornithine and L-lysine for oxygen consumption and product formation in comparison to holo-AMO. AMO has shown to be highly specific to its substrate, L-ornithine as other NMOs are. When L-Lysine was used as the substrate it was able to stimulated oxygen consumption, but no hydroxylated product was formed as was seen with AfSidA(20) and KtzI(42). Data suggests that L-lysine act as a non-substrate effector.

One of the most interesting observation found concerning the steady-state kinetics of AMO was the issue of coenzyme preference for holo-AMO and apo-AMO. While both are, able to consume oxygen with either NADPH or NADH, Table 9 indicates that there is a clear difference between the apparent binding affinity for NADPH and NADH. This trend is also seen within the product formation assay. From this result, it is indicated that NADPH is the preferred coenzyme for holo-AMO and NADH for apo-AMO, based on lower K_M values.

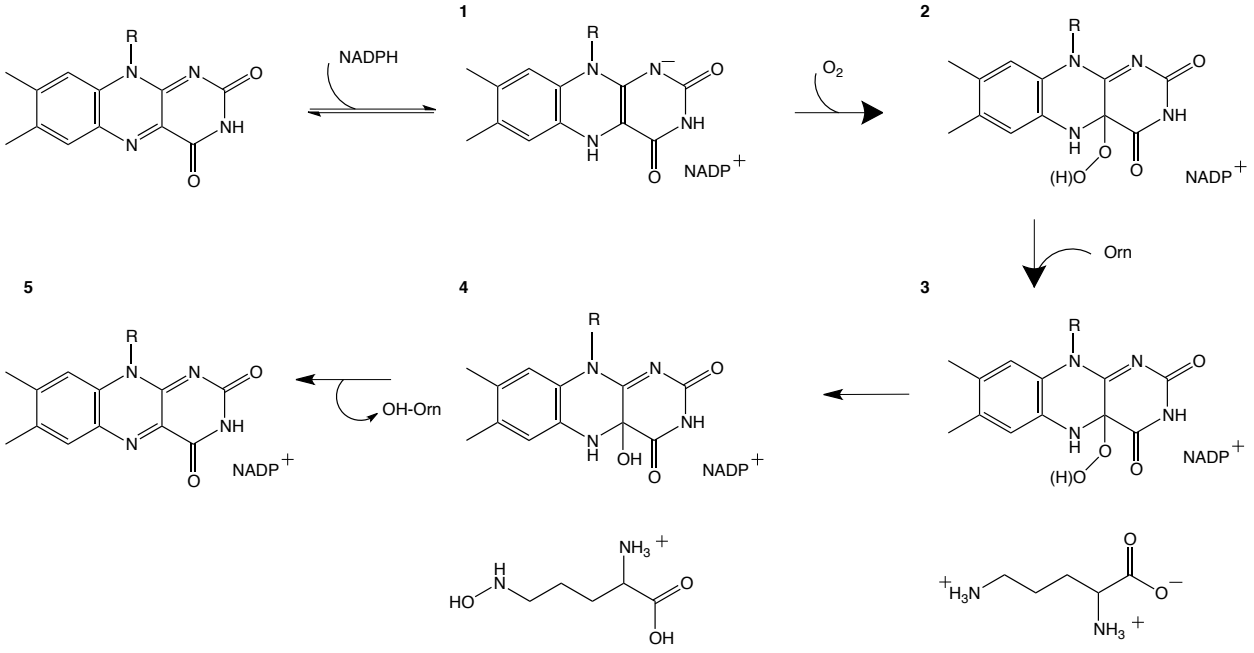

Scheme 1: Proposed kinetic mechanism of hydroxylation of L-Orn catalyzed by AfSidA 1. The reaction starts with the reduction of the flavin by NADPH (2). Then, molecular oxygen reacts with the reduced flavin to form the C_{4a}-oxygenates species intermediate (3). At this point, L-Ornithine binds (4) and follows hydroxylation to N^5-hydroxyornithine (5). Finally, the release of $NADP^+$ completes the catalytic cycle.

Chapter 4. Conclusions and Future Studies

4.1 Inhibition Studies of SidA

In this study, we identified and characterized inhibitors of the enzyme SidA with the aim of blocking the siderophore biosynthesis pathway in *Aspergillus fumigatus*. At first, we screened 973 compounds composed by bioactive properties. Out of the 973 compounds ebselen was validated as an inhibitor of SidA. Seven ebselen derivatives that are commercially available were also analyzed. A substitution from selenium to sulfur in the azole ring lead to the identification and characterization of 2-phenyl-2,3-dihydro-1,2-benzothiazole-3-one (ebsulfur). Ebselen and Ebsulfur displayed an IC_{50} of 10 and 40 μM respectively. This indicates that selenium is playing an important role in the inhibition of SidA activity. When other modifications were made such as change from ketone to amide in the azole ring or removing of a benzene group no inhibition was observed.

To gain further insight on the inhibition mechanism of SidA, we need to conduct crystallization experiments with the compounds. Crystallization studies would provide information on the compound binding site either in the NADPH or Orn pocket and what type of interactions are occurring. Ebsulfur would also be assed for any in cellulo effects as it was done with ebselen. Ebselen did not show to have any effect and it is possible that Ebsulfur would be active.

4.2 Characterization of AMO

In the second part of the thesis we provided kinetic information about the hydroxamate formation in the siderophore albachelin in *Amycolatopsis alba*. We have shown that AMO can be purified with and without the cofactor flavin bound. Using diverse techniques, we have characterized and determined AMO steady-state and rapid rate kinetics parameters, including catalytic rates, substrate binding affinities and coenzyme specificities. The catalytic mechanism follow a similar pattern as other L-ornithine N-hydroxylating monooxygenase such as PvdA and SidA in which the enzyme undergoes two half-reactions (Scheme 2). The characterization of the two-half reaction was done using product formation, oxygen consumption and stopped- flow spectrophotometry. It was revealed that AMO prefers the amino acid L-ornithine as the substrate. In respect to coenzymes, apo-AMO prefers NADH while holo-AMO prefers NADPH due to lower binding affinities.

Further characterization of AMO would be used to give more insight into the mechanism of action of this enzyme. Studies would include monitoring flavin re-oxidation in the presence and absence of substrate to see if there is formation of intermediates. As well as the role of $NADP^+$ in the catalytic cycle. Experiments would include using the oxygen consumption assay to analyze if $NADP^+$ causes inhibition of AMO. Crystal structure determination of AMO would also provide useful information on the conformational changes during coenzyme binding or any structural arrangements that occur during catalysis. As well as give insight into the active site of apo-AMO and holo-AMO and their coenzyme preferences. Overall, a known three-dimensional structure will help give information to the L-ornithine N^5-oxygenases class of enzymes due to limited known structures of this class.

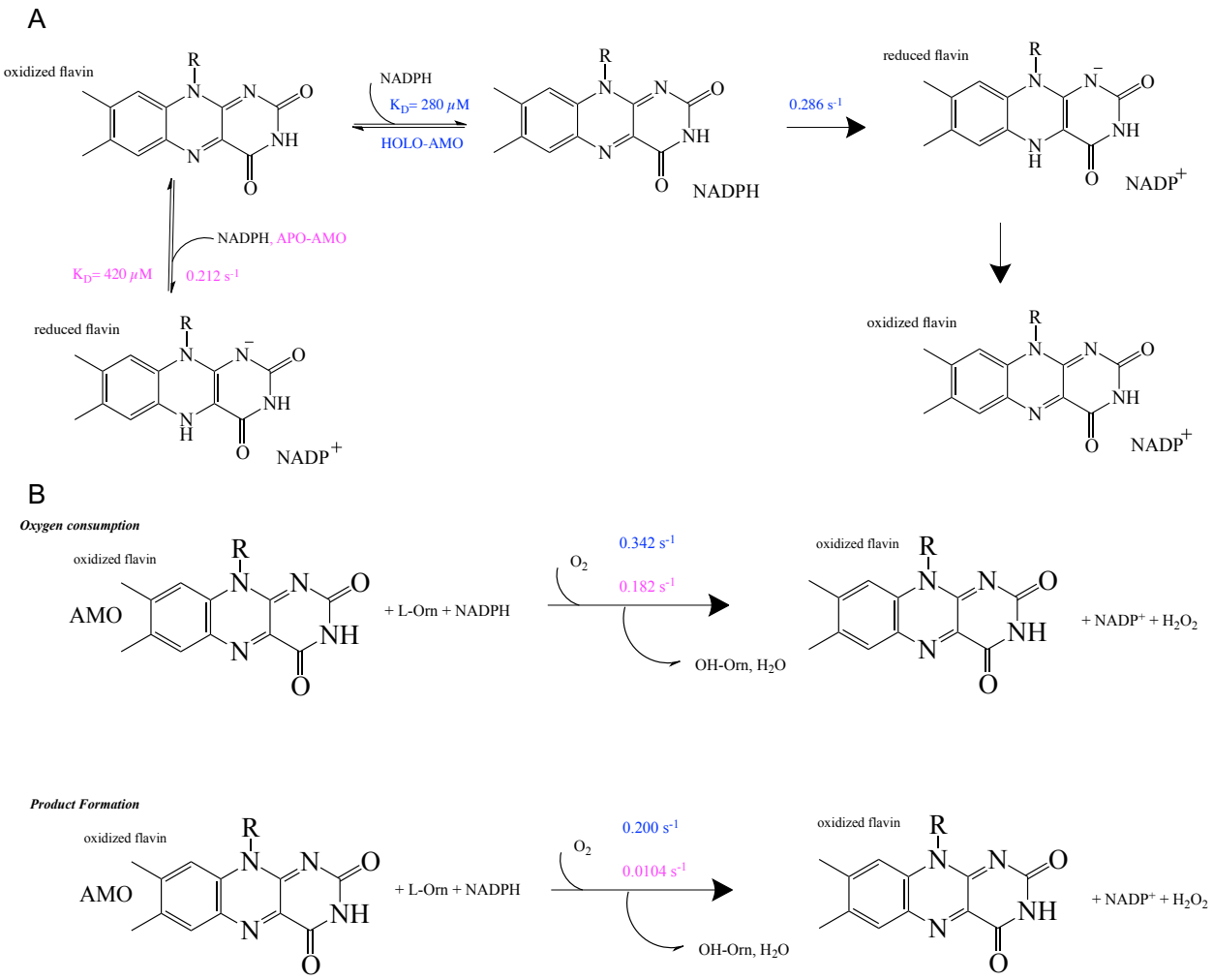

Scheme 2. Proposed catalytic mechanism for the flavin monooxygenase AMO. (A) Pre-steady state kinetics and (B) Steady-state kinetics. Holo-AMO and Apo-AMO kinetics represented in blue and pink respectively.

Reference:

1. Franceschini, S., van Beek, H. L., Pennetta, A., Martinoli, C., Fraaije, M. W., and Mattevi, A. (2012) Exploring the Structural Basis of Substrate Preferences in Baeyer-Villiger Monooxygenases: INSIGHT FROM STEROID MONOOXYGENASE. *The Journal of Biological Chemistry* **287**, 22626-22634
2. Nordlund, P., and Eklund, H. (1993) Structure and Function of the Escherichia coli Ribonucleotide Reductase Protein R2. *Journal of Molecular Biology* **232**, 123-164
3. Schmitz, R. A., Albracht, S. P. J., and Thauer, R. K. (1992) A molybdenum and a tungsten isoenzyme of formylmethanofuran dehydrogenase in the thermophilic archaeon Methanobacterium wolfei. *European Journal of Biochemistry* **209**, 1013-1018
4. Torres Pazmiño, D. E., Winkler, M., Glieder, A., and Fraaije, M. W. (2010) Monooxygenases as biocatalysts: Classification, mechanistic aspects and biotechnological applications. *Journal of Biotechnology* **146**, 9-24
5. Huijbers, M. M. E., Montersino, S., Westphal, A. H., Tischler, D., and van Berkel, W. J. H. (2014) Flavin dependent monooxygenases. *Archives of Biochemistry and Biophysics* **544**, 2-17
6. Sutton, W. B. (1957) MECHANISM OF ACTION AND CRYSTALLIZATION OF LACTIC OXIDATIVE DECARBOXYLASE FROM MYCOBACTERIUM PHLEI. *Journal of Biological Chemistry* **226**, 395-405
7. Joosten, V., and van Berkel, W. J. H. (2007) Flavoenzymes. *Current Opinion in Chemical Biology* **11**, 195-202
8. Ruangchan, N., Tongsook, C., Sucharitakul, J., and Chaiyen, P. (2011) pH-dependent Studies Reveal an Efficient Hydroxylation Mechanism of the Oxygenase Component of p-Hydroxyphenylacetate 3-Hydroxylase. *The Journal of Biological Chemistry* **286**, 223-233
9. Ballou, D. P., Entsch, B., and Cole, L. J. (2005) Dynamics involved in catalysis by single-component and two-component flavin-dependent aromatic hydroxylases. *Biochemical and Biophysical Research Communications* **338**, 590-598
10. Massey, V. (1994) Activation of molecular oxygen by flavins and flavoproteins. *Journal of Biological Chemistry* **269**, 22459-22462
11. Entsch, B., and van Berkel, W. J. (1995) Structure and mechanism of para-hydroxybenzoate hydroxylase. *The FASEB Journal* **9**, 476-483
12. Massey, V. (2000) The Chemical and Biological Versatility of Riboflavin. *Biochemical Society Transactions* **28**, 283-296
13. van Berkel, W. J. H., Kamerbeek, N. M., and Fraaije, M. W. (2006) Flavoprotein monooxygenases, a diverse class of oxidative biocatalysts. *Journal of Biotechnology* **124**, 670-689
14. Entsch, B., Cole, L. J., and Ballou, D. P. (2005) Protein dynamics and electrostatics in the function of p-hydroxybenzoate hydroxylase. *Archives of Biochemistry and Biophysics* **433**, 297-311
15. Moonen, M. J. H., Fraaije, M. W., Rietjens, I. M. C. M., Laane, C., and van Berkel, W. J. H. (2002) Flavoenzyme-Catalyzed Oxygenations and Oxidations of Phenolic Compounds. *Advanced Synthesis & Catalysis* **344**, 1023-1035

16. Malito, E., Alfieri, A., Fraaije, M. W., and Mattevi, A. (2004) Crystal structure of a Baeyer–Villiger monooxygenase. *Proceedings of the National Academy of Sciences of the United States of America* **101**, 13157-13162
17. Nijvipakul, S., Wongratana, J., Suadee, C., Entsch, B., Ballou, D. P., and Chaiyen, P. (2008) LuxG Is a Functioning Flavin Reductase for Bacterial Luminescence. *Journal of Bacteriology* **190**, 1531-1538
18. Tinikul, R., Pitsawong, W., Sucharitakul, J., Nijvipakul, S., Ballou, D. P., and Chaiyen, P. (2013) The Transfer of Reduced Flavin Mononucleotide from LuxG Oxidoreductase to Luciferase Occurs via Free Diffusion. *Biochemistry* **52**, 6834-6843
19. Sheng, D., Ballou, D. P., and Massey, V. (2001) Mechanistic Studies of Cyclohexanone Monooxygenase: Chemical Properties of Intermediates Involved in Catalysis. *Biochemistry* **40**, 11156-11167
20. Chocklett, S. W., and Sobrado, P. (2010) Aspergillus fumigatus SidA Is a Highly Specific Ornithine Hydroxylase with Bound Flavin Cofactor. *Biochemistry* **49**, 6777-6783
21. Morrison, E., Kantz, A., Gassner, G. T., and Sazinsky, M. H. (2013) Structure and Mechanism of Styrene Monooxygenase Reductase: New Insight into the FAD–Transfer Reaction(). *Biochemistry* **52**, 10.1021/bi400763h
22. Dong, C., Flecks, S., Unversucht, S., Haupt, C., van Pée, K.-H., and Naismith, J. H. (2005) The structure of tryptophan 7-halogenase (PrnA) suggests a mechanism for regioselective chlorination. *Science (New York, N.Y.)* **309**, 2216-2219
23. Neilands, J. B. (1995) Siderophores: Structure and Function of Microbial Iron Transport Compounds. *Journal of Biological Chemistry* **270**, 26723-26726
24. Haas, H. (2014) Fungal siderophore metabolism with a focus on Aspergillus fumigatus. *Natural Product Reports* **31**, 1266-1276
25. Sandy, M., and Butler, A. (2009) Microbial Iron Acquisition: Marine and Terrestrial Siderophores. *Chemical reviews* **109**, 4580-4595
26. Carrano, C. J., and Raymond, K. N. (1978) Coordination chemistry of microbial iron transport compounds: rhodotorulic acid and iron uptake in Rhodotorula pilimanae. *Journal of Bacteriology* **136**, 69-74
27. Van der Helm D, W. G. (1994) Hydroxamates and polycarbonates as iron transport agents (siderophores) in fungi. . *Metal ions in fungi*, 39-148
28. Renshaw, J. C., Robson, G. D., Trinci, A. P. J., Wiebe, M. G., Livens, F. R., Collison, D., and Taylor, R. J. (2002) Fungal siderophores: structures, functions and applications. *Mycological Research* **106**, 1123-1142
29. Mei, B., Budde, A. D., and Leong, S. A. (1993) sid1, a gene initiating siderophore biosynthesis in Ustilago maydis: molecular characterization, regulation by iron, and role in phytopathogenicity. *Proceedings of the National Academy of Sciences of the United States of America* **90**, 903-907
30. Schrettl, M., Bignell, E., Kragl, C., Sabiha, Y., Loss, O., Eisendle, M., Wallner, A., Arst, H. N., Jr., Haynes, K., and Haas, H. (2007) Distinct Roles for Intra- and Extracellular Siderophores during Aspergillus fumigatus Infection. *PLOS Pathogens* **3**, e128
31. (2008) Siderophores in Fungal Physiology and Virulence. *Annual Review of Phytopathology* **46**, 149-187

32. Kleinkauf, H., and Von Döhren, H. (1996) A Nonribosomal System of Peptide Biosynthesis. *European Journal of Biochemistry* **236**, 335-351
33. Hameed, S., Pal, R., and Fatima, Z. (2015) Iron Acquisition Mechanisms: Promising Target Against Mycobacterium tuberculosis. *The Open Microbiology Journal* **9**, 91-97
34. Wertheimer, A. M., Verweij, W., Chen, Q., Crosa, L. M., Nagasawa, M., Tolmasky, M. E., Actis, L. A., and Crosa, J. H. (1999) Characterization of the angR Gene of Vibrio anguillarum: Essential Role in Virulence. *Infection and Immunity* **67**, 6496-6509
35. Meyer, J. M., Neely, A., Stintzi, A., Georges, C., and Holder, I. A. (1996) Pyoverdin is essential for virulence of Pseudomonas aeruginosa. *Infection and Immunity* **64**, 518-523
36. Hissen, A. H. T., Wan, A. N. C., Warwas, M. L., Pinto, L. J., and Moore, M. M. (2005) The Aspergillus fumigatus Siderophore Biosynthetic Gene sidA, Encoding l-Ornithine N(5)-Oxygenase, Is Required for Virulence. *Infection and Immunity* **73**, 5493-5503
37. Plattner, H. J., and Diekmann, H. (1994) Enzymology of siderophore biosynthesis in fungi. *Metal ions in fungi. New York: Marcel Decker*, 99-117
38. Romero, E., Fedkenheuer, M., Chocklett, S. W., Qi, J., Oppenheimer, M., and Sobrado, P. (2012) Dual role of NADP(H) in the reaction of a flavin dependent N-hydroxylating monooxygenase. *Biochimica et Biophysica Acta (BBA) - Proteins and Proteomics* **1824**, 850-857
39. Csaky, T. Z. (1948) On the estimation of bound hydroxylamine in biological materials. *Acta Chemica Scandinavica* 450-454
40. Robinson, R., and Sobrado, P. (2011) Substrate Binding Modulates the Activity of Mycobacterium smegmatis G, a Flavin-Dependent Monooxygenase Involved in the Biosynthesis of Hydroxamate-Containing Siderophores. *Biochemistry* **50**, 8489-8496
41. Binda, C., Robinson, R. M., Martin del Campo, J. S., Keul, N. D., Rodriguez, P. J., Robinson, H. H., Mattevi, A., and Sobrado, P. (2015) An Unprecedented NADPH Domain Conformation in Lysine Monooxygenase NbtG Provides Insights into Uncoupling of Oxygen Consumption from Substrate Hydroxylation. *The Journal of Biological Chemistry* **290**, 12676-12688
42. Neumann, C. S., Jiang, W., Heemstra, J. R., Gontang, E. A., Kolter, R., and Walsh, C. T. (2012) Biosynthesis of Piperazic Acid via N(5)-Hydroxy-ornithine in Kutzneria spp. 744. *Chembiochem : a European journal of chemical biology* **13**, 972-976
43. Forneris, F., Orru, R., Bonivento, D., Chiarelli, L. R., and Mattevi, A. (2009) ThermoFAD, a Thermofluor®-adapted flavin ad hoc detection system for protein folding and ligand binding. *FEBS Journal* **276**, 2833-2840
44. Martín del Campo, J. S., Vogelaar, N., Tolani, K., Kizjakina, K., Harich, K., and Sobrado, P. (2016) Inhibition of the Flavin-Dependent Monooxygenase Siderophore A (SidA) Blocks Siderophore Biosynthesis and Aspergillus fumigatus Growth. *ACS Chemical Biology*
45. Schrettl, M., Bignell, E., Kragl, C., Joechl, C., Rogers, T., Arst, H. N., Haynes, K., and Haas, H. (2004) Siderophore Biosynthesis But Not Reductive Iron Assimilation Is Essential for Aspergillus fumigatus Virulence. *The Journal of Experimental Medicine* **200**, 1213-1219
46. Zhang, J.-H., Chung, T. D. Y., and Oldenburg, K. R. (1999) A Simple Statistical Parameter for Use in Evaluation and Validation of High Throughput Screening Assays. *Journal of Biomolecular Screening* **4**, 67-73

47. Hansen, S. H., Olsson, A., and Casanova, J. E. (1995) Wortmannin, an Inhibitor of Phosphoinositide 3-Kinase, Inhibits Transcytosis in Polarized Epithelial Cells. *Journal of Biological Chemistry* **270**, 28425-28432
48. Heinekamp, T., Schmidt, H., Lapp, K., Pähtz, V., Shopova, I., Köster-Eiserfunke, N., Krüger, T., Kniemeyer, O., and Brakhage, A. A. (2015) Interference of Aspergillus fumigatus with the immune response. *Seminars in Immunopathology* **37**, 141-152
49. Ip, C., and Ganther, H. E. (1992) Comparison of selenium and sulfur analogs in cancer prevention. *Carcinogenesis* **13**, 1167-1170
50. Kodani, S., Komaki, H., Suzuki, M., Hemmi, H., and Ohnishi-Kameyama, M. (2015) Isolation and structure determination of new siderophore albachelin from Amycolatopsis alba. *BioMetals* **28**, 381-389
51. Kelley, L. A., Mezulis, S., Yates, C. M., Wass, M. N., and Sternberg, M. J. E. (2015) The Phyre2 web portal for protein modeling, prediction and analysis. *Nat. Protocols* **10**, 845-858
52. Grabski, A., Mehler, M., and Drott, D. (2005) The Overnight Express Autoinduction System: High-density cell growth and protein expression while you sleep. *Nature Methods* **2**, 233-235
53. Studier, F. W. (2014) Stable Expression Clones and Auto-Induction for Protein Production in E. coli. in *Structural Genomics: General Applications* (Chen, Y. W. ed.), Humana Press, Totowa, NJ. pp 17-32
54. Macheroux, P. (1999) UV-Visible Spectroscopy as a Tool to Study Flavoproteins. in *Flavoprotein Protocols* (Chapman, S. K., and Reid, G. A. eds.), Humana Press, Totowa, NJ. pp 1-7
55. Tomlinson, G., Cruickshank, W. H., and Viswanatha, T. (1971) Sensitivity of substituted hydroxylamines to determination by iodine oxidation. *Analytical Biochemistry* **44**, 670-679
56. Gillam, A. H., Lewis, A. G., and Andersen, R. J. (1981) Quantitative determination of hydroxamic acids. *Analytical Chemistry* **53**, 841-844
57. Robinson, R. M., Rodriguez, P. J., and Sobrado, P. (2014) Mechanistic studies on the flavin-dependent N6-lysine monooxygenase MbsG reveal an unusual control for catalysis. *Archives of Biochemistry and Biophysics* **550–551**, 58-66
58. Romero, E., Robinson, R., and Sobrado, P. (2012) Monitoring the Reductive and Oxidative Half-Reactions of a Flavin-Dependent Monooxygenase using Stopped-Flow Spectrophotometry. *Journal of Visualized Experiments : JoVE*, 3803
59. Setser, J. W., Heemstra, J. R., Walsh, C. T., and Drennan, C. L. (2014) Crystallographic Evidence of Drastic Conformational Changes in the Active Site of a Flavin-Dependent N-Hydroxylase. *Biochemistry* **53**, 6063-6077
60. Meneely, K. M., Barr, E. W., Bollinger, J. M., and Lamb, A. L. (2009) Kinetic mechanism of ornithine hydroxylase (PvdA) from Pseudomonas aeruginosa: substrate triggering of O(2) addition but not flavin reduction. *Biochemistry* **48**, 4371-4376